M3LW-24OR0402037
ANL/LWRS-24/1

Light Water Reactor Sustainability Program

Effect of thermal aging on microstructure and stress corrosion cracking behavior of an Alloy 152 1st layer butter weldment

Bogdan Alexandreanu, Yiren Chen, Xuan Zhang and Wei-Ying Chen
Nuclear Science and Engineering Division, Argonne National Laboratory

September 2024
U.S. Department of Energy
Office of Nuclear Energy

ANL/LWRS-24/1

Effect of thermal aging on microstructure and stress corrosion cracking behavior of an Alloy 152 1st layer butter weldment

LWRS milestone Report Number: M3LW-24OR0402037

Nuclear Science and Engineering Division
Argonne National Laboratory

About Argonne National Laboratory
Argonne is a U.S. Department of Energy laboratory managed by UChicago Argonne, LLC under contract DE-AC02-06CH11357. The Laboratory's main facility is outside Chicago, at 9700 South Cass Avenue, Argonne, Illinois 60439. For information about Argonne and its pioneering science and technology programs, see www.anl.gov.

ANL/LWRS-24/1

Effect of thermal aging on microstructure and stress corrosion cracking behavior of an Alloy 152 1st layer butter weldment

LWRS milestone Report Number: M3LW-24OR0402037

Bogdan Alexandreanu, Yiren Chen, Xuan Zhang and Wei-Ying Chen

Nuclear Science and Engineering Division, Argonne National Laboratory

September 2024

This page intentionally left blank

ABSTRACT

Nickel-based Alloy 690 and the associated weld Alloys 52 and 152 are typically used for nozzle penetrations in replacement heads for pressurized water reactor (PWR) vessels, because of their excellent overall resistance to general corrosion and environmental degradation, primarily stress corrosion cracking (SCC). However, many of the existing PWRs are expected to operate for 40-80 years. Likewise, water-cooled small modular reactors (SMRs) will use Ni-Cr alloys and are expected to receive initial operating licenses for 60 years. Hence, the thermal stability of Ni-Cr alloys is critical for the long-term performance of both existing and advanced nuclear power plants, and possibly spent fuel storage containers. The objective of this research is to understand the microstructural changes occurring in high-Cr, Ni-based Alloy 152 weldments during long time exposure to the reactor operating temperatures, and the effect of these changes on the service performance. One area of particular concern is the potential for long range ordering (LRO), *i.e.* formation of the intermetallic Ni_2Cr phase under prolonged exposure to reactor temperatures and/or irradiation, which can increase strength, decrease ductility, and cause dimensional changes or lead to in-service embrittlement of components made with these alloys. Hence, this research focused on the microstructural evolution and the SCC response of Alloy 152 under accelerated thermal aging. The materials studied involved three heats of Alloy 152 used to produce a dissimilar metal weld (DMW) joining an Alloy 690 plate to an Alloy 533 low alloy steel (LAS) plate, thermally aged at three different temperatures (370°C, 400°C and 450°C) for different durations up to 75,000h (equivalent to 60 years of reactor service). The microstructural characterization by means of synchrotron X-ray conducted in small, 0.2 mm - step line scans in the high-deformation regions of the weld root – covering areas spanning from the weld heat affected zone (HAZ) in Alloy 690 to the weld and weld butter on LAS - did not show evidence of LRO in any of the three Alloy 152 heats aged at 370°C and 450°C to an equivalent of 60 years of service. However, the first weld butter layer has high levels of deformation and is highly susceptible to SCC even in its non-aged condition. Nanohardness testing confirmed the extreme hardening with aging (ΔHV $\cong$ 100) at two locations within this weldment. In absence of LRO, hardening is suspected to be due to thermally-induced Cr carbide precipitation and coarsening. Testing in a primary water environment of the 1st layer of Alloy 152 weld butter aged at 370°C to a 60-year service equivalent revealed a fatigue and corrosion fatigue crack growth responses similar to those measured on the un-aged alloys. Similarly, the SCC CGR response of the aged weld butter does not appear to show a deterioration in performance, however, the difficult-to-test weldment geometry may affect the test results.

TABLE OF CONTENTS

LIST OF FIGURES

LIST OF TABLES

ABBREVIATIONS

ANL	Argonne National Laboratory
APS	Advanced Photon Source
ASTM	American Society for Testing and Materials
BPR	Back Pressure Regulator
BWR	Boiling Water Reactor
CGR	Crack Growth Rate
CL	Constant Load
CMTR	Certified Material Test Report
CSL	Coincident Site Lattice
CT	Compact Tension
DO	Dissolved Oxygen
DMW	Dissimilar Metal Weld
ECP	Electrochemical Potential
EDX	Energy Dispersive X-ray Spectroscopy
EPRI MRP	Electric Power Research Institute Materials Reliability Program
GBE	Grain Boundary Engineering
GTAW	Gas Tungsten Arc Welding
HAZ	Heat Affected Zone
HX	Heat Exchanger
IG	Intergranular
LAS	Low Alloy Steel
LWR	Light Water Reactor
NRC	Nuclear Regulatory Commission
PPU	Partial Periodic Unloading
PWR	Pressurized Water Reactor
PWHT	Post Weld Heat Treatment
PWSCC	Primary Water Stress Corrosion Cracking
SCC	Stress Corrosion Cracking
SEM	Scanning Electron Microscopy
SMAW	Shielded Metal Arc Welding
SS	Stainless Steel
S	Side
T	Transverse
TC	Thermocouple
TG	Transgranular
WOL	Weld Overlay
WPS	Weld Procedure Specification

ACKNOWLEDGMENTS

This research was supported through the U.S. Department of Energy's Light Water Reactor Sustainability program, Materials Research Pathway. Materials Research Pathway lead: Dr. Xiang (Frank) Chen.

1 Introduction

Alloy 690 and the associated weld Alloys 52 and 152 are Nickel-based alloys with high Cr contents typically used for nozzle penetrations in replacement heads for pressurized water reactor (PWR) vessels, because of their increased resistance to stress corrosion cracking (SCC) relative to Alloys 600, 82, and 182 [1, 2]. Many of these reactors are expected to operate for 40-80 years. Likewise, advanced water-cooled small modular reactors (SMRs) will use these Ni-Cr alloys in their primary systems and are expected to receive initial operating licenses for 60 years. For spent fuel containers, the desired lifetime is 10,000 years. Hence, the thermal stability of Ni-Cr alloys is critical for the long-term performance of nuclear plants and possibly spent fuel storage containers.

One area of concern is that the long term exposure to reactor operating temperatures can result in long range ordering (LRO), *i.e.* formation of the intermetallic Ni_2Cr phase which can lead to in-service embrittlement of Ni-Cr components. Research with binary Ni-Cr model alloys [3] has found that LRO promotes SCC, with an SCC crack growth rate (CGR) 1,000x larger than the non-ordered version of the alloy. However, Fe plays a key role in the development of LRO. It is not clear at this time whether LRO occurs in commercial Ni-Cr alloys containing significant Fe. The addition of Fe was found to hinder the LRO formation in Ni-Cr alloys [4].

Perhaps the most comprehensive study on LRO of Alloy 690 was conducted by Framatome/ EdF [5, 6]. One of the main findings of this study was that an Alloy 690 heat with 7.2 wt. % Fe requires 70,000 h to develop LRO at 420°C, while ordering had not occurred in Alloy 690 with 10.4 wt. % Fe aged for 70,000 h at the same temperature. 20% added cold-work was found to decrease the time to develop LRO slightly, to 60,000h. More recently, Huotilainen et al. found significant increases in hardness in two of the four heats aged up to 10,000h at 400°C [7]. The two heats that hardened had a lower Fe content than the heats that did not harden (9.53 and 9.3 wt. % vs. 10.37 and 10.04 wt. %). The latter observation is consistent with the formation of LRO as its kinetics is known to decrease with the increase of Fe concentration, however, Fe levels of up to 10 wt. % were found not to impede the LRO formation [4]. Nevertheless, the hardening reported in two of the four heats is similar to that resulting from 15-20% added cold work [7], thus, may have the potential to elevate their SCC susceptibility, leading to CGRs comparable to those typical of Alloy 600. Another remarkable recent study has found that LRO precipitation under proton irradiation was observed for the first time, in alloys C22, 625, 625P, 625D, 725, and 690 [8]. The Fe level in the Alloy 690 heat was 10.38 wt. %, and the irradiation was conducted at 360°C with 2 MeV protons to a damage level of 2.5 dpa.

Overall, the research to date on the effect of aging in Ni-based alloys seems to have been focused almost exclusively on the base alloys, and primarily on model alloys as the investigators sought to gain a fundamental understanding of the mechanisms in play. As a result, research on commercial heats has been extremely scarce and limited to microstructural examinations. As noted previously, with the notable exception of the study by Young et. al [3] on model alloy Ni-33Cr, the effects of those microstructural changes on the SCC response have not been evaluated.

The need for an assessment of the long-term aging effects on the performance in Alloy 690 and associated weldments was identified as a research gap in the Light Water Reactor Sustainability (LWRS) stakeholders report for 2020 [9], and was recognized as a strategic research need by both industry [2, 10] and regulators [11]. Hence, a research program was initiated at Argonne in 2020 to address that need and bridge the gap between the microstructural evolution and service performance. In order to study the effect of aging on performance, ANL produced an Alloy 152 dissimilar metal weld joining Alloy 690 and Alloy 533 low alloy steel (LAS) in 2011, identical to the one developed and produced for the US NRC program in 2010, which was then aged at different temperatures up to 75,000h over the following nine years, to 30 and 60-year service equivalents. This creates the opportunity to examine the effects of aging on service performance in several pedigreed alloys that have been characterized and tested extensively at ANL and worldwide in the un-aged condition over the past decade.

In its first year, the Argonne program focused on the microstructural evolution and the SCC response of Alloy 690 under accelerated thermal aging and irradiation conditions [12]. In addition to the aged Alloy 690, the study also involved specimens neutron-irradiated in the BOR-60 reactor up to 40 dpa. For aged Alloy 690 specimens, hardness was found to increase with aging time, however, the microstructural characterization by means of synchrotron X-ray did not find evidence of LRO. The microstructural characterization of neutron-irradiated specimens by TEM found no evidence of LRO either. Testing in a primary water environment of Alloy 690 specimens aged to a 60-year service equivalent revealed a fatigue and corrosion fatigue crack growth responses similar to those measured on the un-aged alloy. The SCC CGR response was also low. Overall, the two Alloy 690 heats investigated in this work, aged up to 60-year service equivalents or exposed to neutron irradiation up to 40 dpa, did not exhibit a detectable deterioration in microstructure or performance.

The subsequent research was focused on the microstructural evolution and the SCC response of Alloy 152 under accelerated thermal aging. Three weld heats aged at 370°C and 450°C equivalent to 60 years of service were analyzed by Synchrotron X-ray Diffraction (XRD), and no ordering was observed [13]. However, the SCC response of the 60-year aged specimen appeared to show a deterioration [13]. In order to confirm these findings, a finer scan of XRD evaluation was conducted in the highly deformed root region of the weld, covering areas spanning from the weld heat affected zone (HAZ) in Alloy 690 to the weld metal and weld butter on LAS [14]. In order to confirm the previous findings on SCC response, two additional Alloys 152 heats aged to a 60-year service equivalent were tested in a primary water environment.

Chapter 2 describes the weld mockup used in the aging study, including the materials of fabrication, the schematic design of the welds, and the weld fabrication processes. One of the objectives for this weldment was that the materials and welding parameters should be representative of those used for actual welds used in service. Chapter 2 also presents the equipment used in the microstructural examinations. The crack growth testing equipment and experimental approach are also presented. ANL generally followed a well-established testing protocol that has been employed for a number of years and was reported in previous ANL reports.

Chapter 3 provides findings of the microstructural examinations and the results of the crack growth rate tests. Complete CGR data sets are provided as a function of testing conditions, and presented as crack advance vs. time plots.

Chapter 4 provides a discussion of the testing results in the framework provided by the well-established fatigue and corrosion fatigue behavior for these alloys, as well as the industry-proposed disposition curves for crack growth [1]. Finally, Chapter 5 gives a summary of the main findings and conclusions.

2 Experimental

This section describes the alloys used in this study, the equipment used for microstructural analysis, the configuration of test specimens for CGR testing, and the CGR test apparatus and experimental approach.

2.1 Alloys

The alloys used in this work came from a weldment that was aged at 370, 400, and 450°C to 30-year and 60-year service equivalents. Since the microstructural investigation was focused on LRO, a model alloy Ni-33Cr – with known susceptibility to LRO - was also included in the investigation.

2.1.1 Alloy 152 weld produced by ANL (Alloy 690 to Alloy 533 Grade B Joint)

The research presented in this report focuses on the aged Alloy 152 which was part of a weldment, hence, for completeness, this section presents all the component materials and steps undertaken to produce the weldment.

The Alloy 690 (Heat NX3297HK12) was received from Nuclear Alloy Corp. in a plate form that was 6.4-cm (2.25-in.) thick x 7.6-cm (3-in.) wide x 86.4-cm (34-in.) long. The designation for the metallurgical condition of the as-received plate was MIL-DTL-24802. To reach this condition, the alloy was vacuum-induction-melted, electro-slag-remelted, hot-rolled, de-scaled, and annealed at 1038°C (1900°F) for 2 h, then air-cooled. The chemical composition provided by the vendor, as well as that determined at ANL by inductively-coupled plasma optical emission spectrometry (ICP-OES), is reported in Table 1.

Table 1 Chemical composition (wt. %) of Alloy 690 (Heat NX3297HK12) plate.

Alloy ID (Heat)	Analysis	C	Mn	Fe	S	P	Si	Cu	Ni	Cr	Ti	Nb	Co
A 690WC (NX3297HK12)	Vendor	0.03	0.20	9.9	<0.001	-	0.07	0.01	59.5	29.5	-	-	-
	ANL	0.04	0.33	8.53	0.001	0.003	0.02	0.04	59.67	30.82	0.47	0.01	<0.01

The Alloy 690 plate was used to produce a 3-inch thick Alloy 152 butt weld to SA-533 Gr B class 1 steel (Heat A5466-2 from the Midland reactor lower head [13]) buttered with Alloy 152 filler metal. The geometry of the joint is shown in Figure 1. The joint was designed with a straight edge on the Alloy 690 side to facilitate SCC CGR testing of the Alloy 690 heat affected zone (HAZ). The SMAW welding procedure was qualified to ASME Section IX by ANL Central Shops [16].

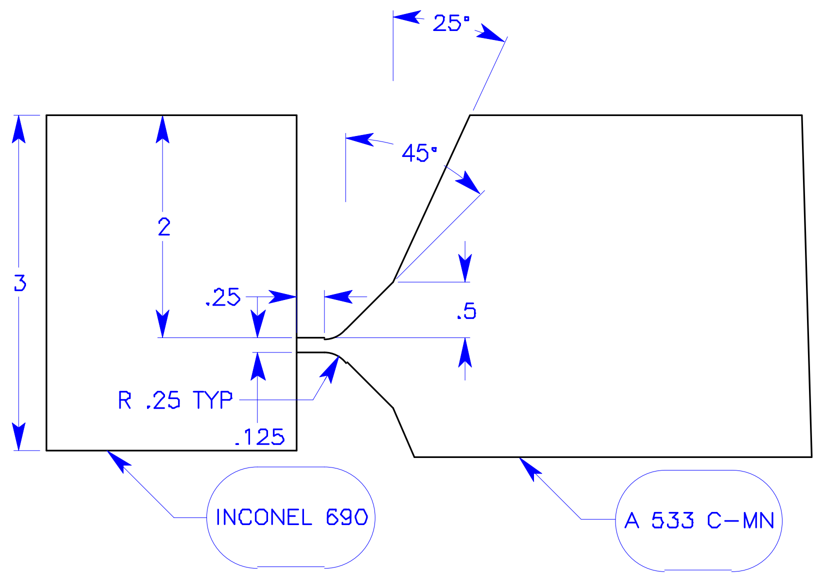

Figure 1 Joint design, Alloy 690 to SA-533 Gr B. Units are in inch.

2.1.1.1 Alloy 152 Weld Buttering

The LAS plate was machined with a bevel on one end. The beveled end was buttered with Alloy 152 F43 filler metal. A record was kept of the number and location of weld passes together with the heat code of the filler metal used, and the welding parameters that were used, Table 2 [16]. This record is shown in [16]. After each layer, a liquid penetrant (LP) check was performed. After buttering, the LAS piece was stress relieved at 1150 ± 25ºF for 3h. The chemical composition of the Alloy 152 filler heat 720129 that was used to produce the first layer of buttering is given in Table 3.

Table 2 Welding process and conditions for various weld passes used for fabricating the Alloy 152 butter

Weld Pass	Process	Filler Metal	Filler Size, in.	Heat Code	Type Polarity	Current, A	Voltage, V	Travel Speed, in./min	Notes
1 – 23	SMAW	Alloy 152, EniCrFe-7	1/8	720129	DCRP	97-102	21 – 23	5	Layer 1 LP
24-44	SMAW	Alloy 152, EniCrFe-7	5/32	146444	DCRP	113-117	25 – 26	5	Layer 2 LP
45-65	SMAW	Alloy 152, EniCrFe-7	5/32	146444	DCRP	113-117	25 – 26	5	Layer 3 LP

DCRP = direct current reverse polarity

Table 3 Chemical composition (wt. %) of Alloy 152 heats used to produce the weld buttering

Alloy ID	Analysis	C	Mn	Fe	S	P	Si	Cu	Ni	Cr	Ti	Nb+Ta	Co
A152 (720129)	CMTR	0.037	3.70	9.28	<0.001	<0.003	0.51	0.01	55.26	28.92	0.12	1.92	<0.01
A152 (146444)	CMTR	0.040	3.56	9.36	<0.001	<0.003	0.46	<0.01	55.25	29.04	0.15	1.84	<0.01

2.1.1.2 Alloy 152 Weldment

The buttered LAS piece described in the previous sub-section was beveled on the buttered edge leaving ¼” of Alloy 152 F43 weld material on the face, and a section of Alloy 690 plate was used to make the opposing part of the butt weld. A double bevel J-grove weld was produced according to the design shown in Figure 1, and the number and location of weld passes together with the heat code of the filler metal used, as well as the welding parameters are given in Table 4. The root pass of the weld and back grind was LP tested, and the final weld surface was also LP tested. The final weld was radiographed per ASME Section IX. The resulting weld along with its component heats is shown in Figure 2 and Figure 3. The chemical composition of the Alloy 152 filler heat WC04F6 that was used to complete the butt weld is given in Table 5.

Table 4 Welding process and conditions for various weld passes used for fabricating the A152 butt weld

Weld Pass	Process	Filler Metal	Filler Size, in.	Heat Code	Type Polarity	Current, A	Voltage, V	Travel Speed, in./min	Notes
1 – 8	SMAW	Alloy 152, EniCrFe-7	1/8	720129	DCRP	97-102	21 – 23	5	
9-14	SMAW	Alloy 152, EniCrFe-7	1/8	720129	DCRP	97-102	25 – 26	5	Root LP BG LP
15-26	SMAW	Alloy 152, EniCrFe-7	5/32	146444	DCRP	113-117	25 – 26	5	Final LP
27-76	SMAW	Alloy 152, EniCrFe-7	1/8	WCO4F6	DCRP	97-102	25 – 26	5	Final LP

DCRP = direct current reverse polarity

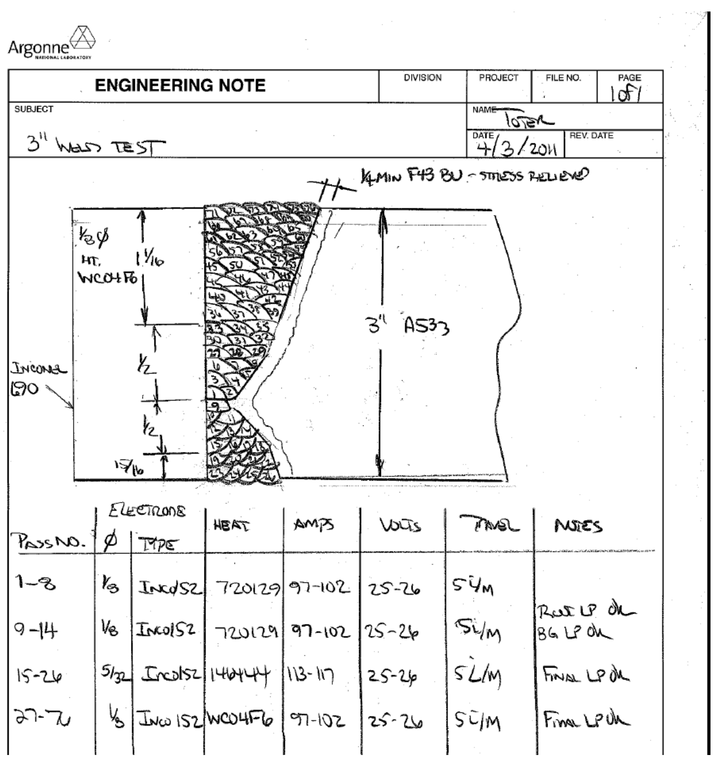

Figure 2 **Schematic of the Alloy 152 weld joining Alloy 690 and Alloy 533 produced for aging in 2011. The weld was produced in an identical fashion using the same materials and procedures used to produce the weld for the US NRC program a year earlier. The table below the weld schematic shows the Alloy 152 weld heats and welding parameters.**

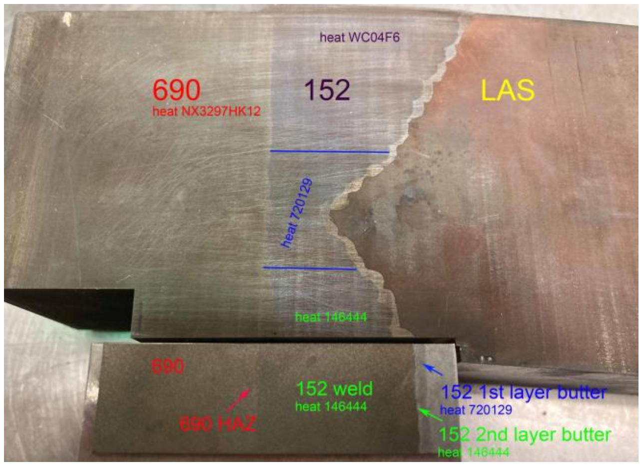

Figure 3 Alloy 152 weld joining Alloy 690 and Alloy 533 aged to a 60-year service equivalent. The three Alloy 152 weld heats are identified.

Table 5 Chemical composition (wt. %) of Alloy 152 heat WC04F6 used to complete the butt weld

Alloy ID (Heat)	Analysis	C	Mn	Fe	S	P	Si	Cu	Ni	Cr	Ti	Nb	Co
A152 (WC04F6)	CMTR	0.048	3.48	10.39	0.003	0.003	0.41	<0.01	55.20	28.70	0.09	1.54	<0.005
	ANL	-	3.88	9.56	-	<0.08	0.52	<0.04	53.70	28.40	0.10	1.80	<0.04

2.1.2 Prior characterization and testing of the un-aged Alloy 152 to Alloy 533 Grade B Joint

One of the main advantages of using the weldment described in this section for an aging study is the existence of a large database for benchmarking. The non-aged material from the sister weldment has been tested extensively at ANL under an US NRC program [17-19] and elsewhere. Some key findings are as follows:

Alloy 690:

- Alloy 690 Heat NX3297HK12 was the original material used by ANL in 2006 to show that 26% cold work promotes SCC growth in Alloy 690. The material was shared with several other laboratories and was tested extensively worldwide. Notably, 11% - the most from any one heat - of the data points in the MRP-386 database [2] were obtained using this heat. Alloy 690 Heat NX3297HK12 has a Fe content below 10 wt. % (9.9 and 8.53 wt. % in two independent measurements, Table 1), so it could be prone to developing LRO under long term exposure. However, the microstructural characterization conducted in this program by means of synchrotron X-ray did not find evidence of LRO in the specimens aged to 60 year of service equivalents [12].

The Alloy 152 weldment was produced with three heats:

- Alloy 152 Weld Heat WC04F6 was used in the upper J-weld. It was tested extensively at ANL [17, 19] and elsewhere, and significant IG SCC was developed routinely in testing, resulting in moderately-high SCC CGRs, Figure 4. It is the most SCC-susceptible weldment in the MRP-386 database [2]. Alloy 152 Weld Heat WC04F6 has a Fe content of 10.39 wt. % (Table 5), so it would be less prone to the formation of LRO under long term exposure.

- Alloy 152 Weld Heat 720129 was used to weld on both sides of the root. It has not been tested as part of the weld, but was tested as the first buttering layer on Alloy 533 LAS. Alloy 152 Weld Heat 720129 has a Fe content of 9.28 wt. % (see Table 3), so it would be prone to LRO formation under long term exposure.
- Alloy 152 Weld Heat 146444 was used to complete the bottom J-weld. It has not been tested as part of the weld, but was tested as the second buttering layer on Alloy 533 LAS. Alloy 152 Weld Heat 146444 has a Fe content of 9.36 wt. % (see Table 3), so it would be prone to LRO formation under long term exposure.

The Alloy 152 butter was produced with two heats (Table 3):

- Alloy 152 Weld Heat 720129 was used as a first layer butter on Alloy 533 LAS. It has been tested extensively at ANL [18] and elsewhere. In SCC CGR testing, this weldment produced fully IG-engaged crack fronts, and very high rates, Figure 5 [18]. The weldment and tested specimens were examined extensively at ANL and worldwide. Alloy 152 Weld Heat 720129 has a Fe content of 9.28 wt. % (see Table 3), so it would be prone to LRO formation under long term exposure.
- Alloy 152 Weld Heat 146444 was used as a second layer butter on the Alloy 533 LAS and was tested in that configuration. This weldment was found to be resistant to SCC. Alloy 152 Weld Heat 146444 has a Fe content of 9.36 wt. % (see Table 3), so it would be prone to LRO formation under long term exposure.

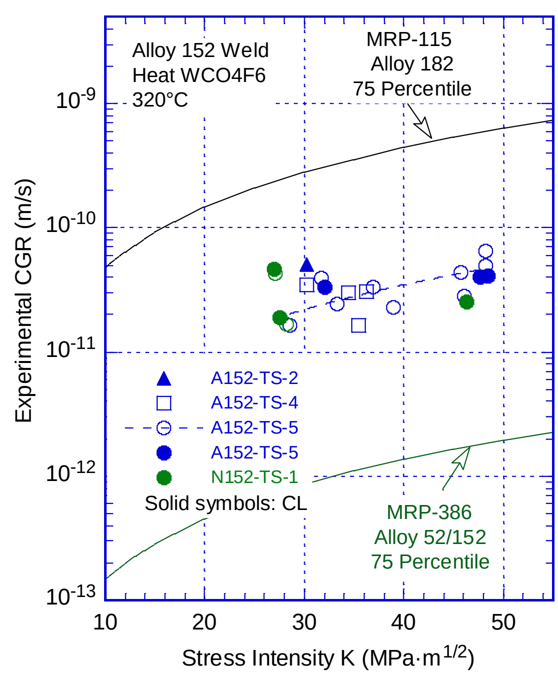

Figure 4 **SCC CGRs for Alloy 152 weld heat WC04F6 [17, 19]. Solid symbols represent SCC CGRs measured under constant load (CL) and open symbols represent SCC CGRs measured under periodic partial unloading (PPU) conditions. The proposed disposition curves for Alloys 182 [1] and 52/152 [2] are included.**

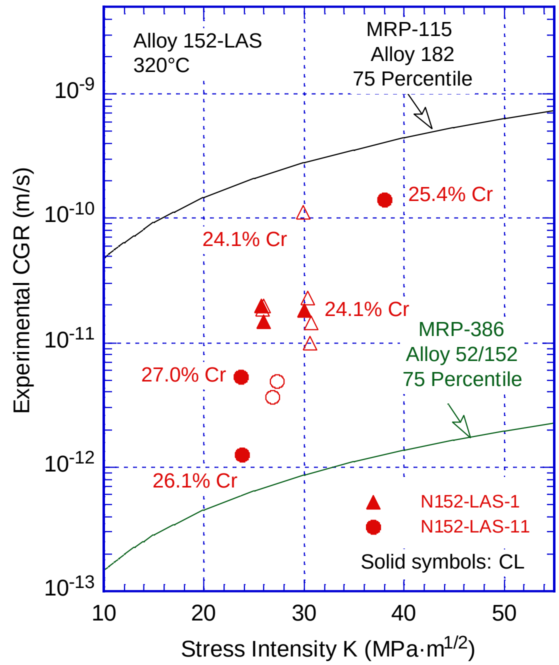

Figure 5 SCC CGRs for 1st layer of Alloy 152-LAS weld heat 720129 [18]. Cr-concentrations measured along the crack path in the regions where the rates were determined are shown in the figures. Solid symbols represent SCC CGRs measured under constant load (CL) and open symbols represent SCC CGRs measured under periodic partial unloading (PPU) conditions. The proposed disposition curves for Alloys 182 [1] and 52/152 [2] are included.

This weldment was also made available to collaborators from Korea, and the microstructure of the Alloy 152 weld, particularly the butter, was examined extensively in the non-aged and intermediate aged conditions [21, 22].

2.1.3 Aging of the Alloy 690 to Alloy 533 Grade B Joint

In order to emulate the thermal exposure at temperatures of 320°C during 30-year and 60-year service lifetimes of a component, this study employed an accelerated aging approach. The aging conditions were determined using the following equation:

$$\frac{t_{aging}}{t_{ref}} = \exp\left[-\frac{Q}{R}\left(\frac{1}{T_{ref}} - \frac{1}{T_{aging}}\right)\right] \qquad (1)$$

where t_{aging} is the aging time (h), t_{ref} is the service time at operation temperature (h), T_{aging} is aging temperature (K), T_{ref} is operation temperature (K), R is the gas constant, and Q is the activation energy.

The 30-year and 60-year year service equivalents were estimated for three aging temperatures (370°C, 400°C, and 450°C) using Eq. (1) with an activation energy of 125 kJ/mol, in excellent agreement with the Framatome/EdF estimate for LRO formation [6], and the results are shown in Figure 6. The figure also includes a photograph of the actual aged weld pieces. The maximum accelerated aging temperature was 450°C to prevent the formation of microstructural phases atypical of normal operating conditions, such as excessive carbides or sigma phases. Specimens are designated by “temperature – service equivalent”, for example specimen “400-Y60” was aged at a temperature of 400°C to reach a 60-year equivalent exposure at 320°C.

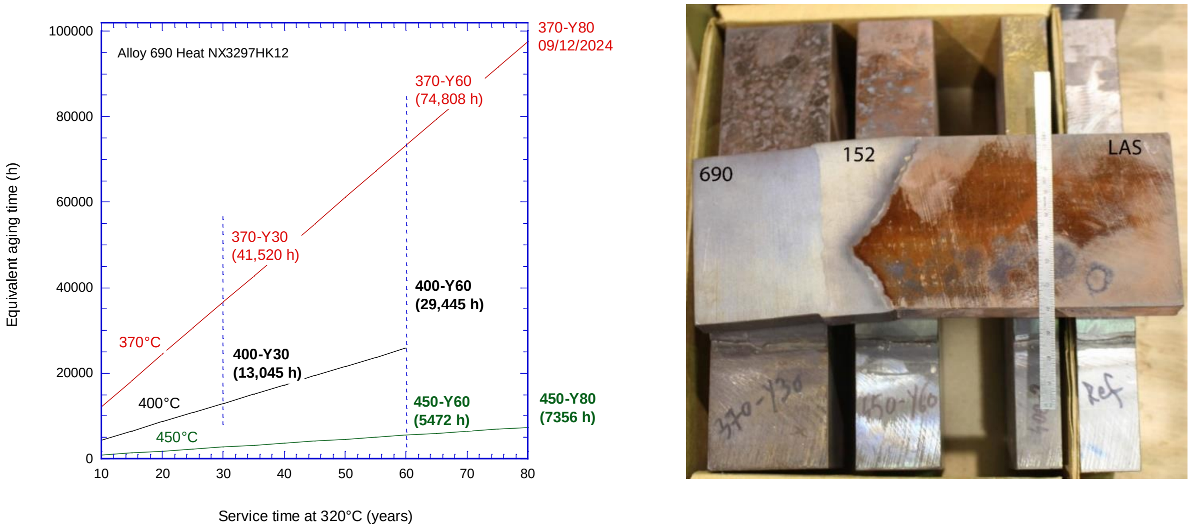

(a) (b)

Figure 6 **(a) Diagram showing the total hours for each aging temperature (370°C, 400°C, and 450°C). Estimates for 30-year and 60-year service equivalents calculated using Eq. (1) with an activation energy of 125 kJ/mol. The diagram also includes the actual aging times. Weld pieces are currently aged to 80-year service equivalent. (b) photograph of the actual pieces of Alloy 152 weld joining Alloy 690 and Alloy 533 that were aged.**

2.1.4 Model Ni-33Cr Alloy

Given that model alloys tend to develop LRO readily (see for example ref. [3]), a piece of model alloy with demonstrated LRO history [24] was obtained for this program from Dr. S.S. Kim of KAERI, Korea. The Ni-33Cr plate was made by vacuum induction melting followed by hot rolling at 1200°C, solution annealing at 1050°C for 1 h and water quenching. At ANL, this solution-annealed alloy was subjected to two different aging treatments at 475°C known to induce LRO [3]. The intent is to use these conditions as reference for the material characterization effort undertaken in this program which involves commercial heats.

2.2 Microstructural Characterization

The microstructural characterization involved hardness testing as well as analytical techniques such as synchrotron diffraction at ANL Advanced Photon Source (APS) focusing on detecting LRO.

2.2.1 X-ray Diffraction at Argonne APS

X-ray diffraction experiments were undertaken at ANL APS with the purpose of detecting LRO in aged Alloy 690 specimens. A similar evaluation has been undertaken previously at ANL APS on a model Ni-33Cr alloy where LRO occurs readily, in as little as 240h under thermal exposure of 475°C [24]. For example, Figure 7 (taken from ref. [24]) shows synchrotron X-ray diffraction peaks from Ni-33Cr alloy in water-quenched and aged conditions. The initial portions of the respective spectra are magnified and are shown as inserts in each figure. In addition to the expected FCC peaks that are present in all alloy conditions, figures (c) and (d) exhibit peaks - indexed with red – typical of Pt_2Mo-type domains. These Pt_2Mo superlattice peaks with d-spacings of 3.76 Å, 3.24 Å, and 2.38 Å were indexed as the (020), (011), and (110) of the body-centered orthorhombic (BCO) structure, and indicate the occurrence of Pt_2Mo-type ordering, i.e., LRO in aged samples.

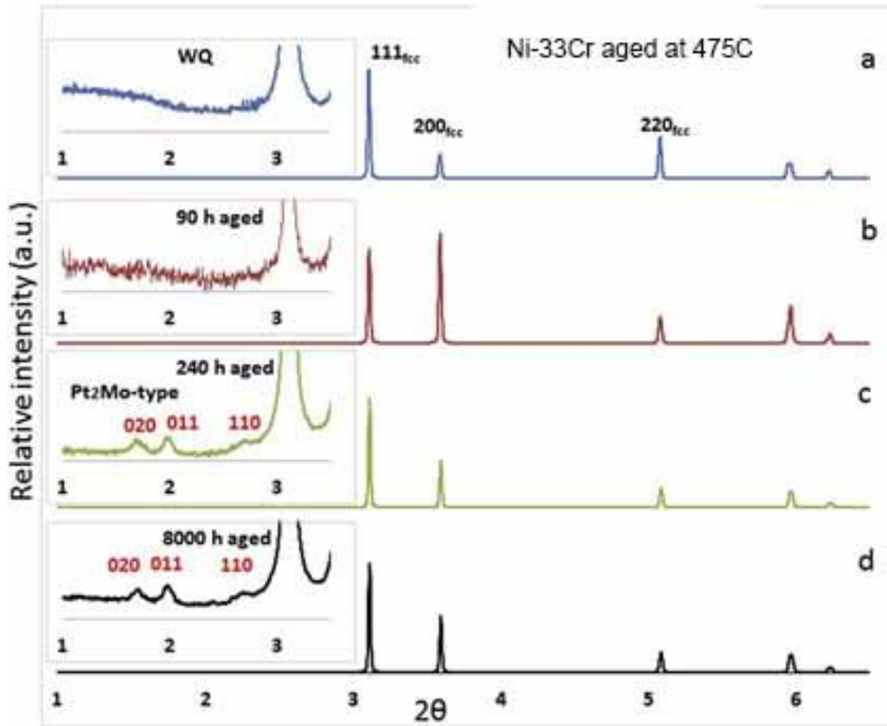

Figure 7 **Synchrotron X-ray peaks from Ni-33Cr alloy (a) water-quenched alloy (b) 90 h aged (c) 240 h aged (d) 8000 h aged. Initial portions of the respective spectra are magnified and are shown as insets. In addition to the FCC peaks that are present in all alloy conditions, (c) and (d) show peaks (indexed with red) from Pt_2Mo-type domains (taken from ref. [24]).**

For the present research, the X-ray diffraction experiment was performed at the 1-ID beamline of the APS, and the experimental details are summarized in Table 6. The detectors were calibrated with a CeO_2 powder sample (NIST standard SRM674b). All the samples were nominally 1-mm thick. For the weld samples, spot measurements were performed at the three Alloy 152 weld heats (refer to Figure 3). Figure 8 is a photo showing the actual beamline setup. At each measurement point, during the exposure, the sample rocked ±1.5°. This approach maximized the diffraction signal coverage in the azimuthal direction that the detector collected to create powder-like diffraction patterns for high-fidelity data analysis. A line scan was also performed for each weld sample, traveling from the Alloy 690 to the LAS with the thinnest weld section; in Figure 8 this corresponds to the right edge of the lead tape that was attached to the sample. For the Ni-33Cr model alloy samples, spot measurements were performed with the same ±1.5° rocking method. The 2D diffraction patterns were transformed into intensity maps of azimuth angles versus radial positions, and were integrated in the azimuthal direction to create the 1-D diffraction profiles for phase identification.

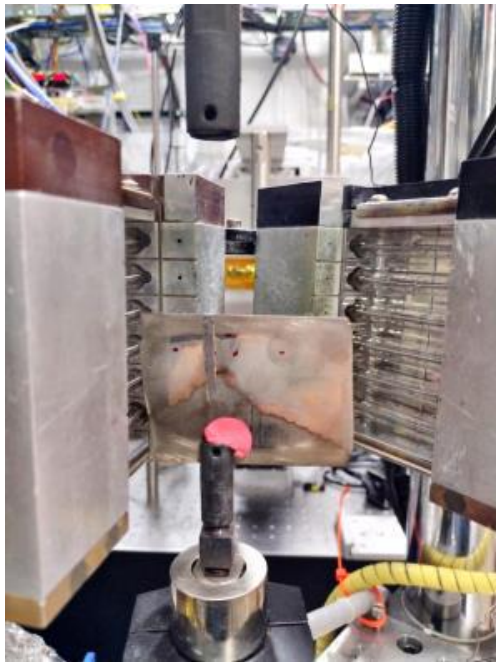

Figure 8 **Experimental setup at the beamline for analyzing the weld material.**

Table 6 **Experimental details for the X-ray diffraction conductucted at ANL APS on aged Alloy 152 and Ni-33Cr specimens.**

Material	Condition	X-ray Energy (keV)	Beam size (mm^2)	Distance sample-detector (mm)
A690 to LAS weld	reference	71.676	0.1 x 0.1	870
A690 to LAS weld	370°C-Y60	71.676	0.1 x 0.1	870
A690 to LAS weld	450°C-Y60	71.676	0.1 x 0.1	870
Ni-33Cr model alloy	reference	71.676	0.1 x 0.1	870
Ni-33Cr model alloy	475°C, 200h	71.676	0.1 x 0.1	870
Ni-33Cr model alloy	475°C, 2000h	71.676	0.1 x 0.1	870

2.2.2 Nanohardness testing

Nanohardness testing was focused on the 1st layer of Alloy 152 butter deposited on the LAS. A Bruker TI Premier nanoindenter was used to measure the nanohardness on polished specimens finished overnight in a Vibromet polisher. Indentation was performed at room temperature with a Berkovich tip and a fixed load of 10000 µN following a 5-2-5 load pattern. The depth for the indents at this load setting was approximately 400 nm. The line profile measurement consisted of three sets of 100 measurements each. The spacing between indents is 2.5 µm. To calculate the nanohardness at each location vs. distance from the fusion line, the indents were imaged optically after the measurement, averaging the three nanohardness measurements at any given distance.

2.3 SCC Crack Growth Rate Testing

2.3.1 Compact tension (CT) Specimens

The tests conducted under this project were performed on ½-T compact tension (CT) specimens; the geometry of the CT specimens is shown in Figure 9. The CGR tests were conducted in simulated PWR environments at 320°C. The testing protocol was in accordance with ASTM E-647, "Standard Test Method for Measurement of Fatigue Crack Growth Rates," [25] and ASTM E-1681, "Standard Test Method for Determining a Threshold Stress Intensity Factor for Environment-Assisted Cracking of Metallic Materials under Constant Load" [26].

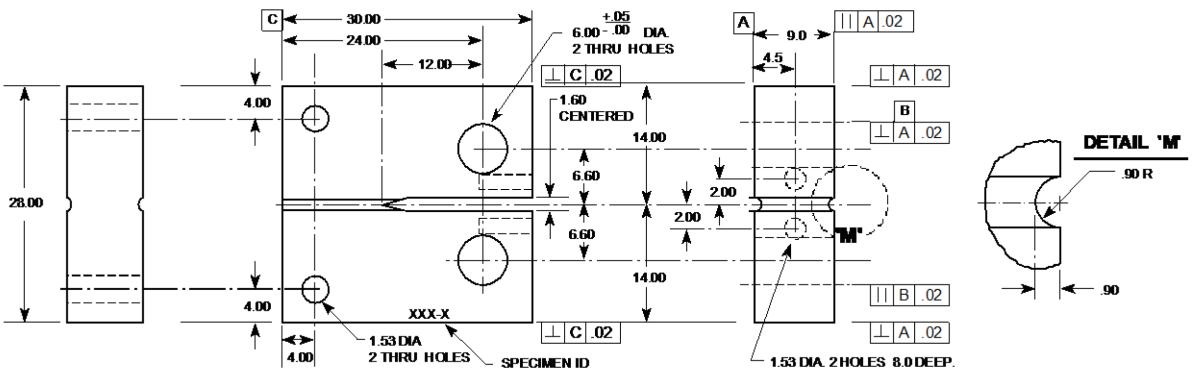

Figure 9 Configuration of the ½-T CT specimen used for this study. Dimensions are in mm.

2.3.2 PWSCC Crack Growth Test Facilities

The CGR tests were conducted in test facilities equipped with either 2 or 6-liter stainless steel (SS) autoclaves. Each system has a suite of calibrated instrumentation, including digitally controlled hydraulic loading and load cells, and an independent water loop to maintain a simulated PWR environment with water chemistry monitoring. The test systems are nearly identical except for the maximum load rating of the test frame and the volume of the autoclave vessel. A detailed description of the test system with the 2-liter autoclave is provided in this section.

The 2-liter autoclave test facility allows test temperatures of up to 350°C. Figure 10 is a photograph showing the entire test system. The servo-hydraulic test frame consists of a load train, an autoclave support frame, and autoclave. The hydraulic actuator is mounted on bottom of the test frame, with the load train components located above it. The load cell is located at the bottom of the pull rod. An Instron Model 8800 system is used to control the load on the specimen. The test temperature is maintained by heater bands mounted on the autoclave body.

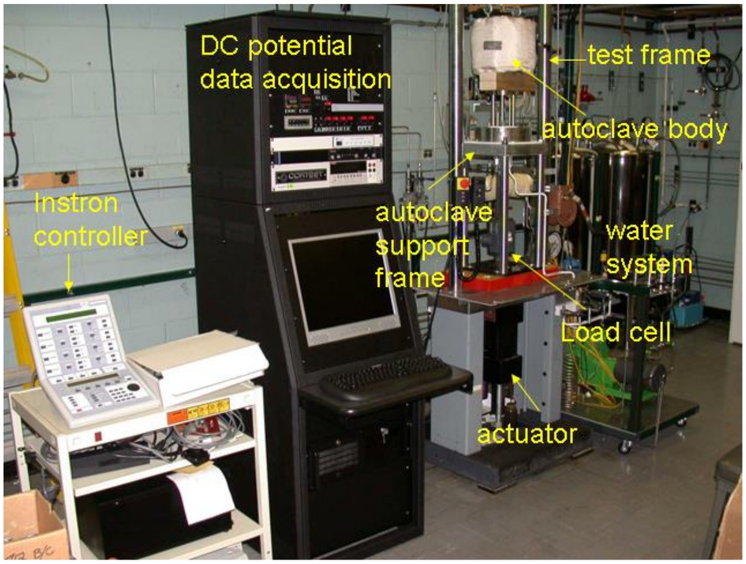

Figure 10 **Layout of the 2-liter SCC test system.**

The autoclave support frame consists of a thick plate supported by four compression rods (Figure 11). The internal load frame that contains the test specimen consists of a top plate supported by three rods. The upper two-piece clevis assembly is fastened to the top plate of the internal load frame, and the lower piece clevis assembly is connected to the pull rod. The specimen to be tested is mounted between the clevises. The specimen and clevises are kept electrically insulated from the load train by using oxidized Zircaloy pins and mica washers to connect the clevises to the rest of the load train. Water is circulated through a port in the autoclave head, which serves both as inlet and outlet. A schematic diagram of the recirculating water system is shown in Figure 12.

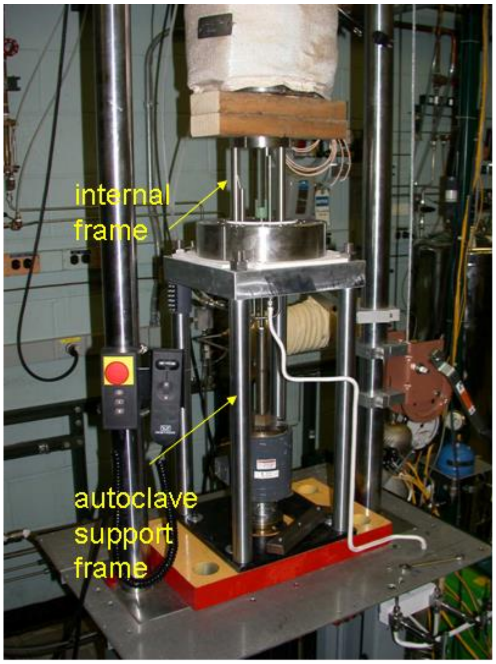

Figure 11 **Photograph of the specimen load train for the 2-liter autoclave.**

The simulated PWR feedwater contains 2 ppm Li as LiOH, 1000 ppm B as HBO_3, ≈2 ppm dissolved hydrogen (≈23 cm^3/kg), and less than 10 ppb dissolved oxygen (DO) [27]. Water is circulated at relatively low flow rates (15-25 mL/min). The test temperature was 320°C.

Crack extensions are monitored by the reversing-direct current (DC) potential difference method, Figure 13. In this method, a constant DC current is passed through the test specimen and the crack length is measured through the changes in the electrical voltage at the crack mouth. The electrical voltage measured across the crack mouth is related to the unbroken crack ligament resistance through the Ohm's law. Thus, as the crack advances, the length of the unbroken ligament decreases and its resistance increases. In short, as the crack advances the voltage measured across the crack mouth increases. Figure 13 shows a typical configuration of a CT specimen instrumented for crack growth measurements by the DC potential method: the current leads are welded on the top and bottom surfaces of the specimen, and potential leads are welded on the front face of the specimen across the machined notch but on diagonal ends. Also, to compensate for the effects of changes in resistivity of the material with time, an internal reference bar of the same material being tested is installed in series, near the test specimen. The voltage readings across the reference bar are used to normalize potential drop measurements for the CT test specimen. The changes in potential drop measurements for the CT test specimen are transformed into crack advance data using correlations developed for the specimen geometry that is tested. In practice, voltage readings are taken successively as the current is reversed, and, typically, 800 voltage readings are needed to generate 1 crack advance data point, approximately every 4 min. with a resolution of approximately 1-2 µm [0.039-0.079 mils].

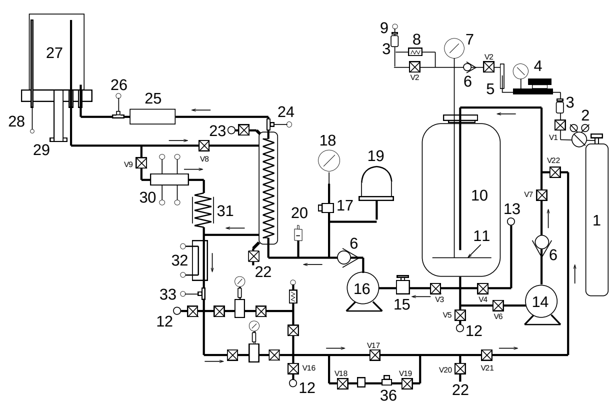

1. COVER GASS SUPPLY TANK
2. TWO-STAGE HIGH-PRESSURE REGULATOR
3. FLASH ARRESTOR
4. LOW-PRESSURE REGULATOR
5. FLOW METER
6. CHECK VALVE
7. COMPOUND VACUUM & PRESSURE GAUGE
8. PRESSURE RELIEF VALVE
9. VENT TO AIR & FLASH ARRESTOR
10. FEEDWATER STORAGE TANK
11. SPARGE TUBE
12. WATER SAMPLE PORT
13. FEEDWATER FILL PORT
14. FEEDWATER TANK RECIRCULATION PUMP
15. SOLENOID VALVE
16. HIGH-PRESSURE PUMP
17. PRESSURE TRANSDUCER
18. HIGH-PRESSURE GAUGE
19. ACCUMULATOR
20. RUPTURE DISC
21. HEAT EXCHANGER (HX)
22. DRAIN
23. SYSTEM BLEED PORT
24. HEAT EXCHANGER OUTLET TC
25. AUTOCLAVE PREHEATER
26. PREHEATER OUTLET TC
27. COMMERCIAL AUTOCLAVE
28. THERMOWELL
29. "BAL SEAL" RETAINER
30. ECP CELL
31. AIR-COOLED COIL
32. WATER COOLED HEAT EXCHANGER
33. BACK-PRESSURE REGULATOR (BPR) INLET TC
34. BPR
35. PH METER
36. CONDUCTIVITY METER

Figure 12 **Schematic diagram of the recirculating 2-liter autoclave system.**

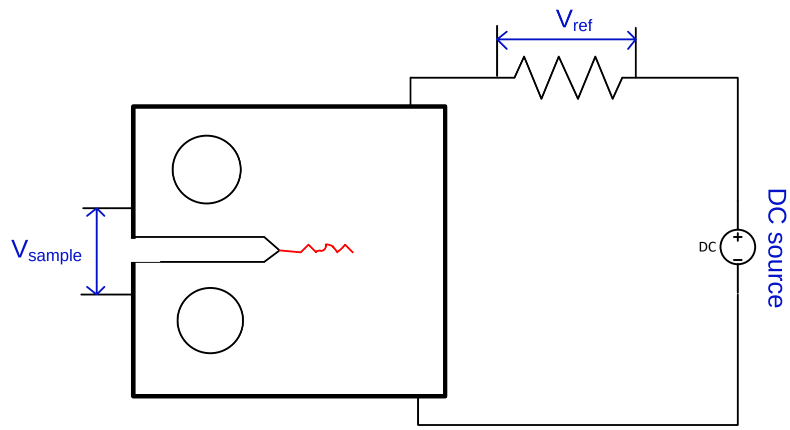

Figure 13 Principle of crack length measurement by the DC potential method.

2.3.2 Test Management of Interface/First Layer Butter Specimens

For tests involving specimens in interface/1st Layer configurations the geometry and microstructure/grain orientation pose additional challenges. In those tests, the dendritic grains are normal to the crack growth plane, hence, in most cases, intergranular SCC is likely to be off-plane, in an orientation that prevents the CGR from being measured by DC potential correctly. However, cases of fast propagation along type II boundaries – normal to the general orientation of the dendritic grains – have been observed. These are the cases where the DC potential can measure the CGR correctly.

Figure 14 illustrates such a 1st layer configuration case. In that test – involving weld overlay (WOL) specimen WOL-ST-1 – the objective was to measure the SCC CGR in the Alloy 52M WOL deposited on Alloy 182. In the figure, the crack propagates in Alloy 52M from right to left in the vicinity of the Alloy 182 (Figure 14a). The direction and geometry of crack propagation is normal to the dendritic grains, and initiating IG SCC cracks tend to follow these boundaries. Therefore, in order to be able to measure SCC growth in the current tests, locations prone to IG SCC propagating in the test crack growth plane had to be identified prior to the SCC CGR determinations. This was accomplished by monitoring the cyclic response and comparing that with prior experience. Specifically, in these tests, the crack was advanced until an environmental enhancement of similar to that obtained in prior tests on Alloy 152 in which the direction of propagation was parallel to the dendritic grains. Of reference are tests conducted at ANL on an Alloy 152 weld that was produced in a symmetric, double-J geometry, described in Ref. [17]. In those tests it was found that environmental enhancement peaks during cyclic with load ratios of $R = 0.5$, and rise time of 600s, and the resulting fracture mode is IG. Based on that experience, a similar level of environmental enhancement in the current tests will be interpreted as IG SCC propagation in a forward direction that can readily be measured by DC potential, and the specimen will be set at constant load.

Following the approach described previously, at some point, approximately 1 mm away from the interface with Alloy 182 (Figure 14a), the cyclic response of specimen WOL-ST-1 was consistent with an IG SCC fracture mode and the specimen was set at constant load for the remainder of the test (location “A” in Figure 14a). The IG SCC crack appears to branch into two directions, “1” and “2”, propagates through the remaining Alloy 52M, and eventually ends on the interface with Alloy 182. This outcome was expected as it had been established in a different test that the interface between the two welds has the fastest SCC CGR, and is thus the most susceptible path [18]. The post-test examination revealed that direction “1” – normal to the dendritic grains - was the dominant crack front. Figure 14b shows the same area after the broken halves were mounted and polished for the EBSD mapping. The IG SCC area of interest is highlighted in Figure 14b. The resulting EBSD map is consistent with a typical, branching IG SCC crack, however, it is not clear what feature(s) could lead to the flat, IG surface observed in direction “1” in the WOL specimen.

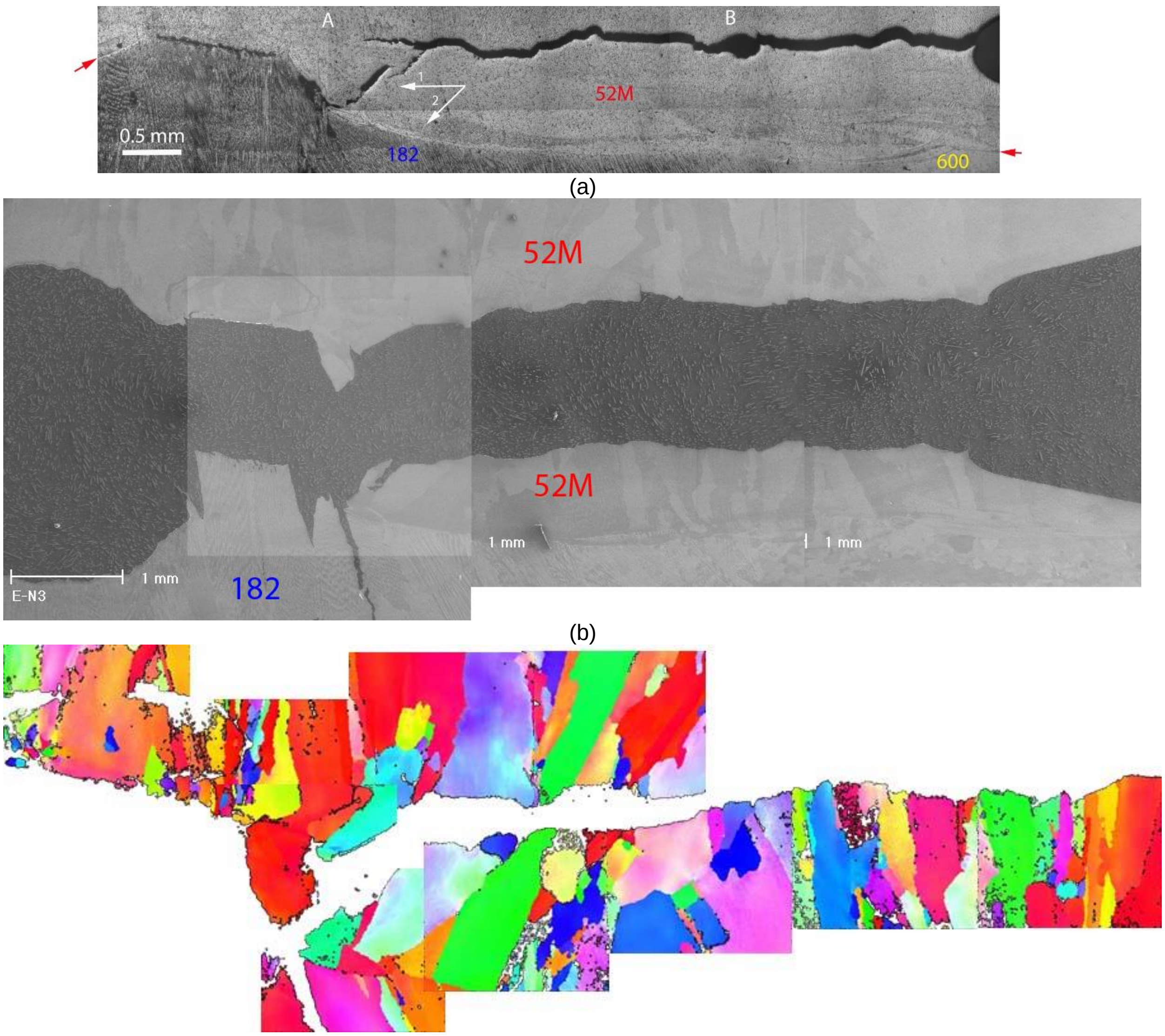

Figure 14 **Cross section of specimen WOL-ST-1: (a) prior to breaking the specimen open, (b) after breaking the specimen open, and (c) EBDS map along the crack path. Crack propagation in from right to left. Taken from Ref. [19].**

Figure 15 illustrates how the approach described previously is used to monitor and manage SCC CGR tests where, in general, one expects significant microstructure changes with crack location. Such microstructures include, as mentioned, first layer butter welds, HAZs, weld repairs, and other defects that are not uniformly distributed. The plot shown in Figure 15 tracks environmental enhancement of cyclic CGRs, defined as CGR_{env}/CGR_{air}, and SCC CGRs on a separate coordinate axis as a function of crack advance. Three horizontal lines provide guides for data analysis:

- "Fatigue response" line shown with black at "1". The $CGR_{env}/CGR_{air}=1$ reflects that the default expectation is that, in most tests, the known fatigue CGRs are reproduced. However, there are cases – such as 1st layer weldments deposited on steels – where the measured CGRs in fatigue are consistently less than expected [17]; nevertheless, the initial fatigue response is extremely useful information: as the test progresses, the investigator compares the subsequent fatigue response with the initial fatigue response to determine whether the crack remained in the material of interest or whether the crack trajectory changed.

- "Environmental enhancement" for two CGRs under loading waveforms with ratios R = 0.5 and rise times of 600s (red dotted line), and 120s (blue dotted line). As explained previously, based on experimental observations involving an IG SCC-susceptible Alloy 152 weld, the resulting fracture mode at the peak level of environmental enhancement (red dotted line) for the waveform with R = 0.5 and rise times of 600s was mostly IG. In a superposition framework for CGRs, the peak total CGR response indicates that a maximum SCC CGR component is added to the constant fatigue CGR.

This viability of the experimental approach described previously was demonstrated when IG SCC susceptible regions were detected in tests involving 1st layer Alloys 52/152 [17]. However, Figure 15 is in fact an example of "no growth". As such, in that test, the known fatigue response was reproduced early in the test, and the response under R = 0.5 and rise times of 600s and 120s are generally consistent with the corrosion fatigue response for this alloy. However, the response in none of the test periods shown in this example (2-11) have reached levels consistent with IG propagation (red dotted line), suggesting that the material at this location is resistant to IG SCC. In this circumstance, it is no surprise that the SCC CGR response measured under constant load in test periods 5 and 14 is in the low 10^{-12} m/s range, essentially, "no growth" conditions.

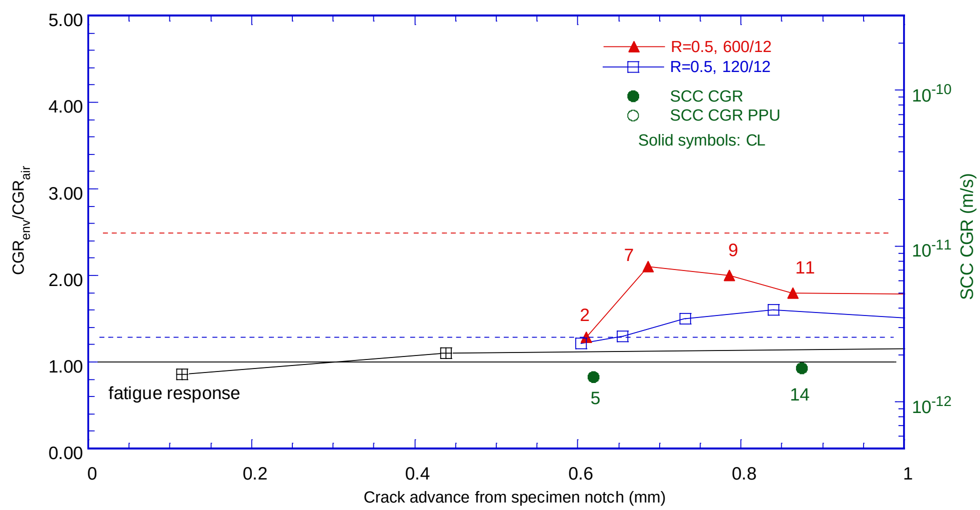

Figure 15 **Example of environmental enhancement of cyclic CGRs and SSC CGRs as a function of crack advance. Taken from Ref. [19].**

For the material of interest in this research, 1st layer of Alloy 152 weld butter deposited on LAS, the feature allowing for crack propagation normal to the dendritic grains is the Type II boundary. Type II boundaries require a ferrite/austenite phase boundary at elevated temperatures to form, i.e., the weld metal solidifies as primary austenite despite the dilution from the base metal, while the LAS solidifies as delta ferrite which then undergoes a transformation first to austenite and then to ferrite/bainite/martensite [31]. Type II boundaries exist parallel to the fusion boundary and are located in the chromium dilution zone, as illustrated in Figure 16 obtained on the un-aged specimen N152-LAS-11. They have been identified in the literature [32] as prone to SCC, owing to the large stress concentrations in their vicinity. Figure 16 shows that both type II and flat high angle boundaries were present in this butter weldment. Additional analysis conducted at ANL over a larger, random area of this 1st layer Alloy 152 butter found that type II/preferentially aligned boundaries are abundant, Figure 17.

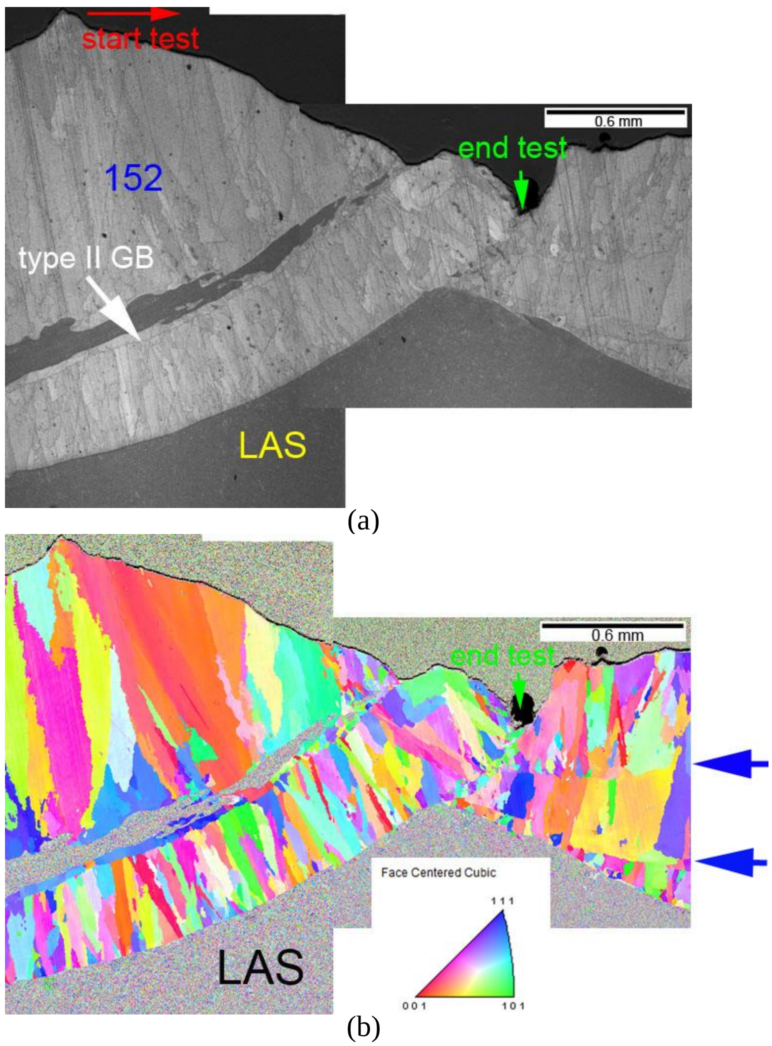

Figure 16 SEM (a) and EBSD (b) map obtained on the side surface of Specimen N152-LAS-11. A red arrow is placed at the specimen notch and indicates the direction of propagation, and green arrows indicate the end of the test. The blue arrows point to sets of aligned boundaries in the next weld bead. Taken from Ref. [20].

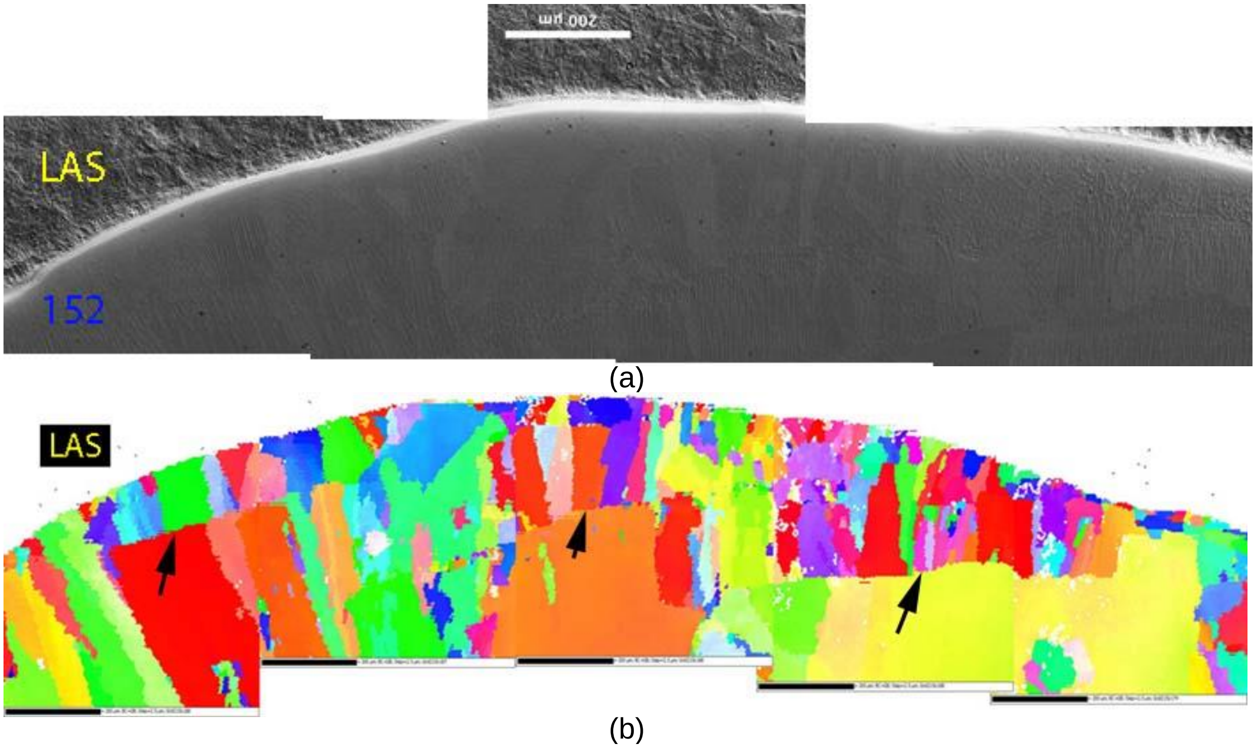

Figure 17 **SEM (a) and EBSD (b) map obtained from Alloy 152-LAS. Several type II/favorably-aligned continuous collection of boundaries are indicated by black arrows. Taken from Ref. [20].**

3 Results

This section describes the findings of the hardness testing, microstructure examination by X-ray diffraction, and the results of SCC CGR testing in a primary water environment. The effects of aging on the 1st Alloy 152 butter layer deposited on LAS was measured by nano-hardness testing. The microstructural examinations focused on reference and weld heats aged at 370°C and 450°C equivalent to 60 years of service (conditions designated 370-Y60 and 450-Y60), Figure 18.

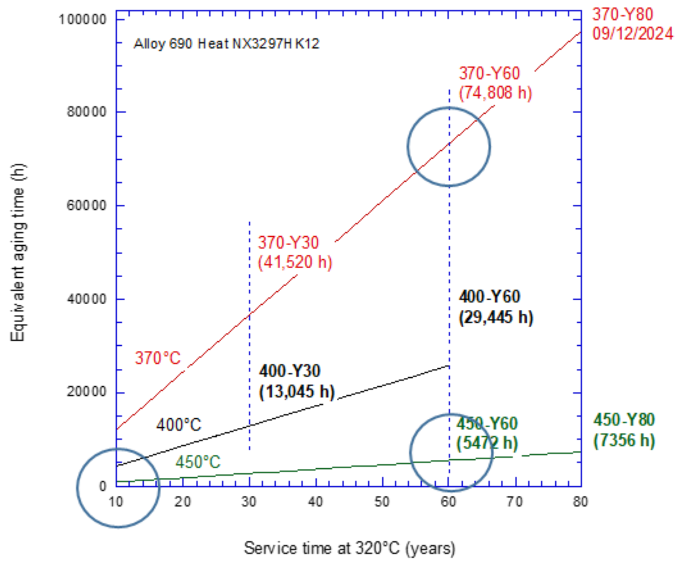

Figure 18 Aging time equivalent vs. service time at 320°C. Conditions of high interest for the microstructural examination are indicated with circles.

3.1 Microstructure

3.1.1 Hardness

The hardness of the non-aged and aged weldments was measured and reported previously [13] and is included here for completeness. The average hardness of the non-aged and two aged conditions - equivalent to 60 years of service, 370-Y60 and 450-Y60 - at select locations in the weld is shown in Figure 19. The load for all measurements was 100 gf, and the standard deviation for each sample hardness average shown in the figure is approximately 14 HV. The hardness map of the reference condition appears to show that the highest levels of deformation are in the weld root region. The overall figure shows similar average hardness values in the non-aged and aged conditions, with the possible exception of the weld root area where hardness appears to increase slightly with aging. The aging temperature, 370°C or 450°C, does not seem to affect the findings. The causes for the hardening – either Cr carbide precipitation or LRO – are both known to increase susceptibility to SCC.

From an SCC susceptibility standpoint, it is also worthy to note the apparently high levels of deformation in the LAS HAZ, although they are not the focus of the current investigation.

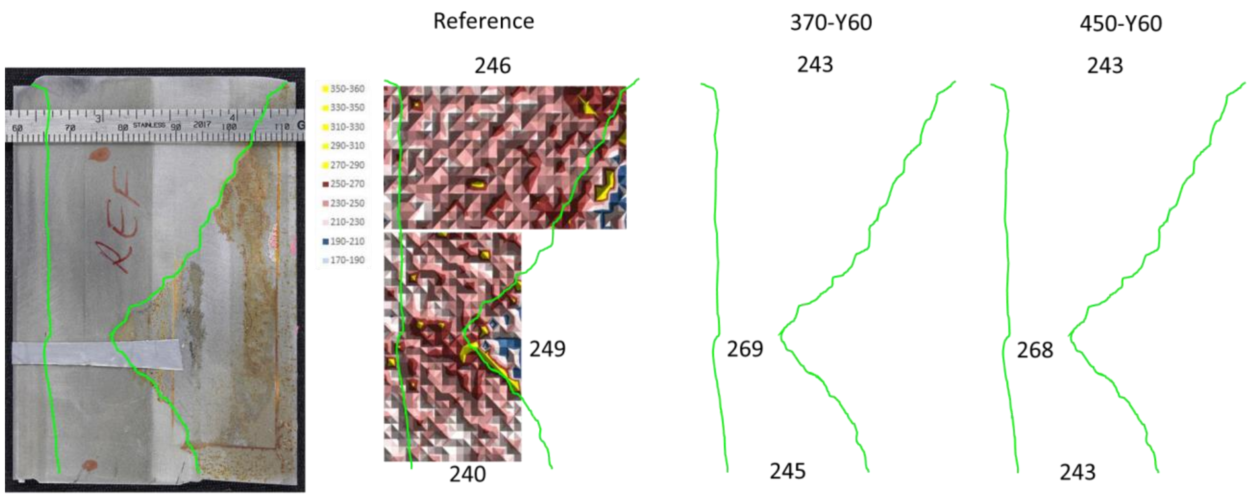

Figure 19 **Average hardness at select locations in the weld for non-aged and two aged conditions equivalent to 60 years of service, 370-Y60 and 450-Y60. The standard deviation for each sample hardness average shown in the figure is approximately 14 HV.**

3.1.2 X-ray Diffraction at Argonne APS

The three Alloy 152 heats - WC04F6, 720129, and 146444 - aged at 370°C and 450°C equivalent to 60 years of service (conditions 370-Y60 and 450-Y60) were examined by X-ray Diffraction (XRD) previously and were found not to display LRO [13]. In order to confirm these findings and expand the measurements to the weld butter layers, and acknowledging the heterogeneity of weldments in in both chemistry and residual stress, it was decided to conduct a "finer" investigation with small step line scans in the weld root region of the weld, known for its high stress. These results have also been reported previously [14], but are included here for completeness.

In that investigation, Figure 20, the reference non-aged condition and the two 60-year aged conditions were evaluated by Synchrotron XRD for LRO over a region spanning areas from the weld HAZ in Alloy 690 to the weld and weld butter on LAS – as indicated by the green arrow.

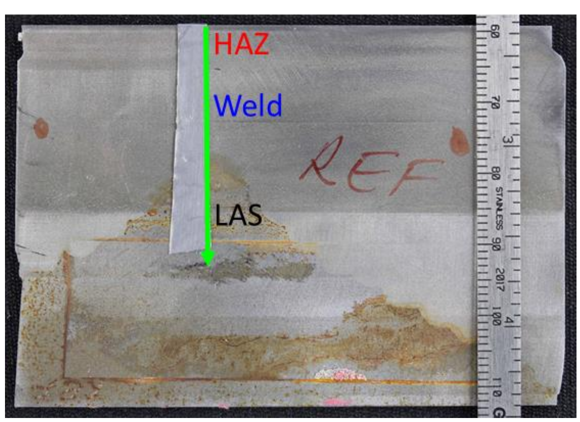

Figure 20 **XRD scanning at with 0.2 mm step was conducted in the weld root region – along the green arrow - spanning the Alloy 690 HAZ, weld rood, and Alloy 152 weld butter deposited on LAS.**

Figure 21 presents the results of the investigation. Aged model Ni-33Cr alloy with known LRO [12] was included for reference in Figure 21a. For the model alloy, in addition to the FCC peaks that are present in all conditions, the aged conditions show peaks - highlighted with green - from Pt_2Mo-type domains. These superlattice peaks with d-spacings of 3.76 Å and 3.24 Å were indexed as the (020) and (011) of the BCO structure, indicating Pt_2Mo-type ordering in these two samples. For the reference and 60-year aged conditions (Figure 21b-d), the XRD line scans conducted along the green arrow Figure 20 spanned a range of alloys in succession (top to bottom): Alloy 690 NX3297HK12 HAZ, Alloy 152 heat 720129 weld, Alloy 152 heat 146444 2nd layer butter, Alloy 152 heat 720129 1st layer butter, and Alloy 533 LAS. For ease of identification, these alloys are color coded as such: red for Alloy 690, blue for Alloy 152 weld, and black for the LAS. The absence of superlattice peaks with d-spacings of 3.24 Å indexed as the (011) of the BCO structure (see Figure 21a for comparison), suggests that the Pt_2Mo-type ordering has not occurred in any of these alloys.

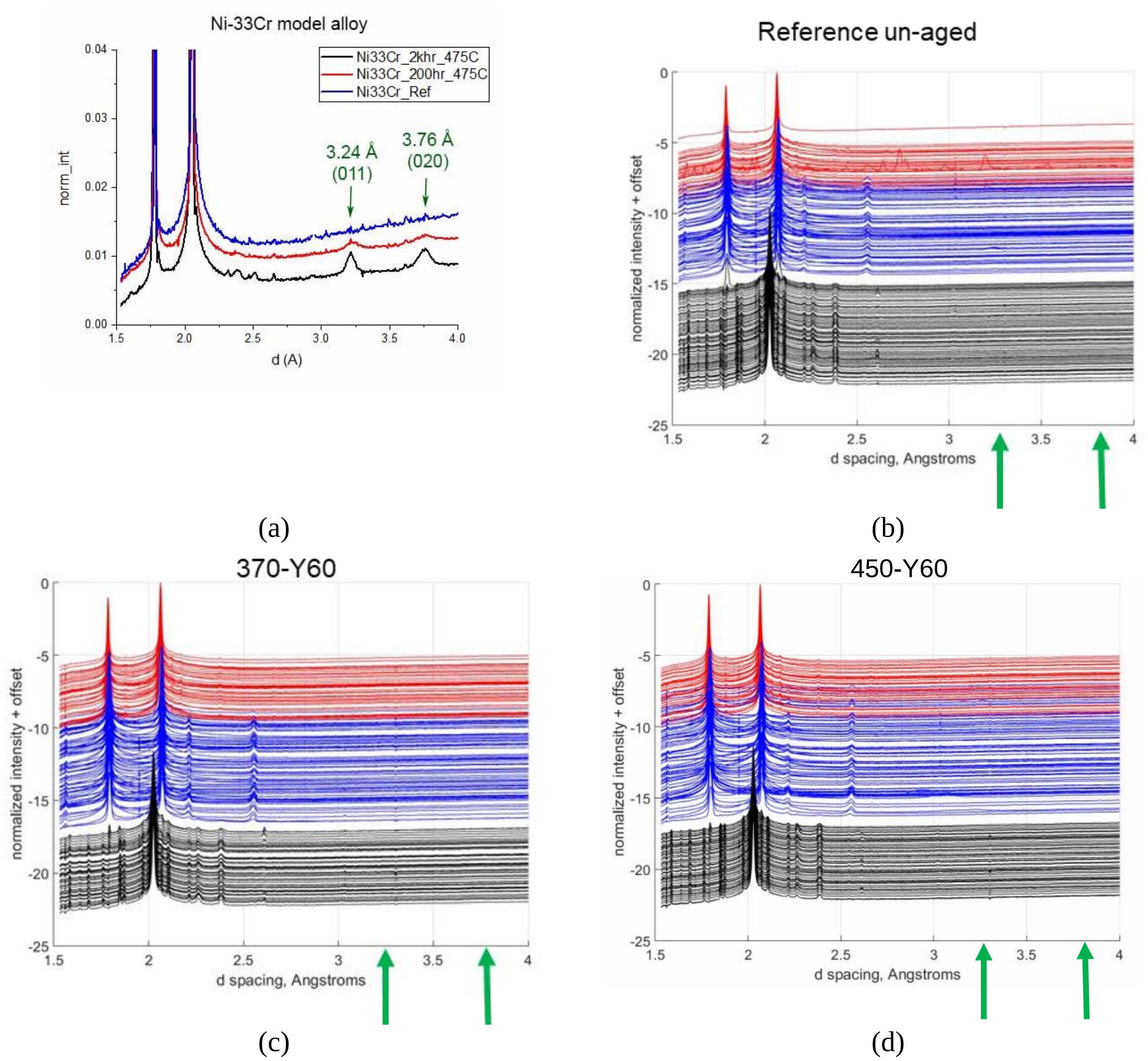

Figure 21 **Synchrotron X-ray peaks from (a) Ni-33Cr alloy, (b) reference un-aged weld, and 60-year aged equivalent conditions (c) 370-Y60, and (d) 450-Y60. Only the aged conditions of model alloy Ni-33Cr show peaks (indexed with green) consistent with Pt_2Mo-type domains.**

3.1.3 Nanohardness of first layer of Alloy 152 butter (Heat 720129) deposited on LAS and aged up to 60-year equivalent service

The nanohardness testing was conducted at two locations, Figure 22. One such location is the “weld root”, as it is the location investigated previously by our Korean collaborators under the I-NERI program [22] and is also the area where the XRD scans described in Figure 20 and Figure 21 were conducted. The second location of interest is the CT location, where such specimens have typically been positioned in previous studies.

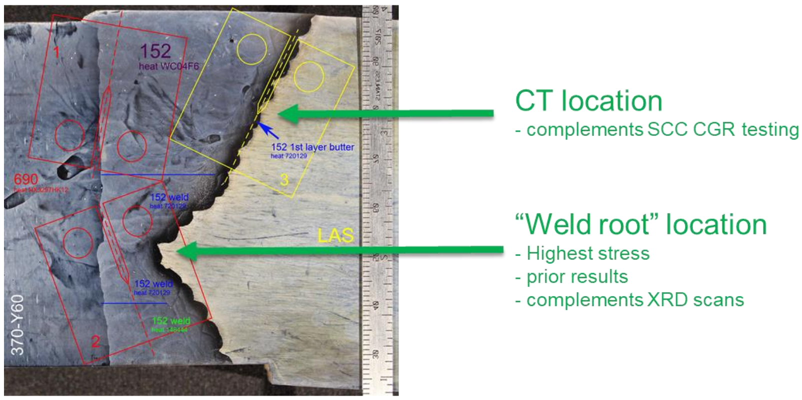

Figure 22 Locations where nanohardness profiles across 1st Layer of Alloy 152 weld butter/LAS interface were obtained: “weld root” and “CT”.

The weld root and CT nanohardness profiles of the reference and 60-year aged conditions (370 and 450°C) are shown in Figure 23. One observes that the weld root hardness of the reference sample first butter layer (Figure 23a) is consistent with the 320 HV value reported by the Korean collaborators in Ref. [22]. All aged and non-aged profiles indicate that hardness is highest near the fusion line. At both locations, aging seems to result in an increase in hardness, however, the aging temperature does not appear to impact the result.

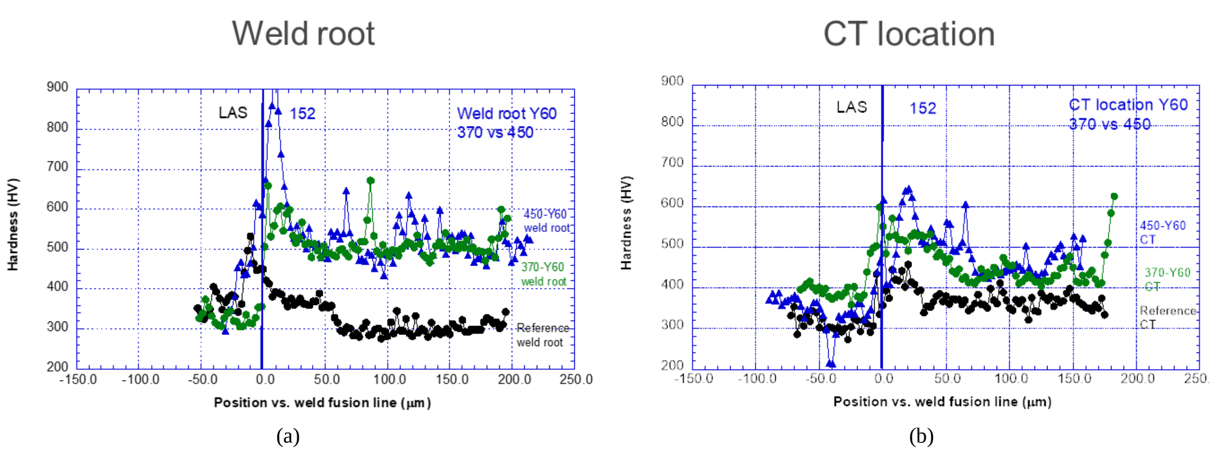

Figure 23 Nanohardness profiles across 1st Layer Alloy 152 weld butter/LAS interface, in both the weld root and CT locations, for reference non-aged and 60-year aged condition at 370°C and 450°C.

Given the very high SCC CGR data (see Figure 5), conducted under a US NRC research program [18], the hardness of the CT location was of high interest. Figure 24 shows that the hardness of that region is indeed very high, even in the unaged specimen. Aging, as described previously, results in substantial hardening, however, the measurements acquired to date, Figure 25, do now show a large difference between the weld root and CT locations. As mentioned previously, the aging conditions, despite the large difference in temperatures and aging times, seem to result in similar levels of hardness.

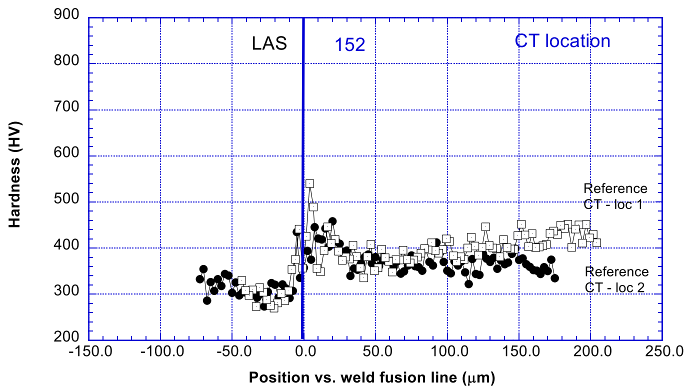

Figure 24 Non-aged nanohardness profiles taken at the CT location across the 1st Layer Alloy 152 weld butter/LAS interface.

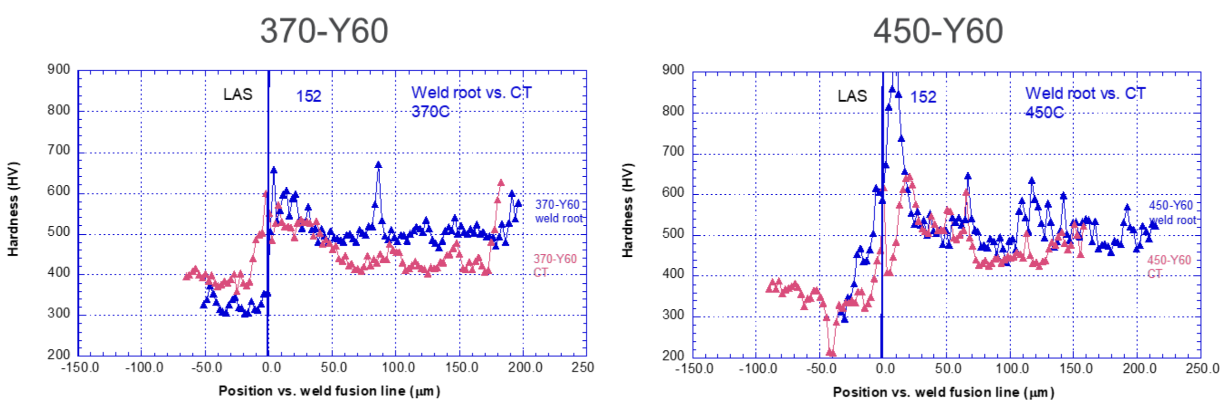

(a) (b)

Figure 25 Nanohardness profiles across 1st Layer Alloy 152 weld butter/LAS interface in the weld root and CT locations for 60-year aged conditions 370 and 450°C comparing the weld root and CT locations in each plot.

3.1.4 Cause of aging-induced hardening

In absence of LRO, determining the cause of hardening became a key objective for this research. The cause of hardening in aged Ni-based was investigated under a US NRC research program at ANL [28], and the outcome is summarized here for completeness. This investigation involved Alloy 690 Heat NX3297HK12 plate in the non-aged and in the 450-Y80 aged condition. These conditions show the largest difference in hardness between the non-aged and an aged condition (HV173 and HV279). The latter hardness value appears to be substantially higher, 61%, than that of the non-aged condition, and is comparable to the hardness increase measured at VTT Finland [7] on two heats of Alloy 690 aged at

400°C. In absence of LRO, hardening was suspected to be due to thermally-induced Cr carbide precipitation. Figure 26 presents Synchrotron XRD data for Alloy 690 Heat NX3297HK12 in the reference un-aged condition and the 450-Y80 aged condition. [29]. The comparison of the Cr-carbide peaks shows that the aged condition peaks are narrower than those for the non-aged condition, as quantitatively described in Table 7. Since the peak widths are inversely proportional to the particle size, the comparison suggests that the carbides have coarsened with aging. The coarsening of grain boundary carbides can lead to higher local stress concentrations, which can cause localized rupture and microcrack formation [30], thus increasing the susceptibility to SCC.

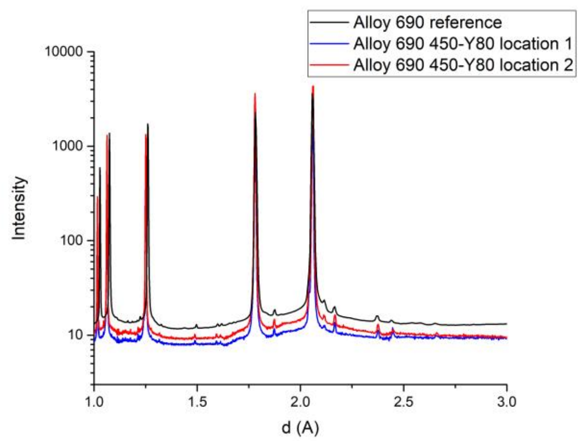

(a)

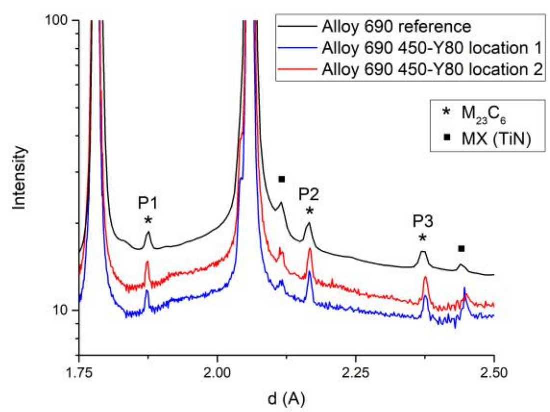

(b)

Figure 26 Synchrotron X-ray peaks from Alloy Heat NX3297HK12 in the reference non-aged condition and aged to 80 years of equivalent service (condition 450-Y80).

Table 7 Comparison of diffraction peak widths for the Cr carbide phase ($M_{23}C_6$).

Specimen	FWHM of P1 (Angstrom)	FWHM of P2 (Angstrom)	FWHM of P3 (Angstrom)
A690 reference	0.009	0.0156	0.0134
A690 450-Y80 location 1	0.006	0.008	0.009
A690 450-Y80 location 2	0.007	0.010	0.010

3.2 PWSCC Crack Growth Rate Testing

3.2.1 SCC CGR testing of Alloy 152 1st layer weld butter Specimen 370-Y60 N152-LAS-11A aged for 74,808 h at 370°C to an equivalent of 60 years of service

The SCC testing of aged specimens involves specimens and heats that have already been tested in the as-welded condition, and have already shown increased susceptibility to SCC, Figure 4 and Figure 5. The SCC CGR testing of aged material is conducted on 1/2T CTs to accommodate more specimens and regions of interest. As such, as shown in Figure 27, from one "slice" of aged weld (370-Y60, aged at 370°C for 74,808 h – equivalent to 60 years of service), an Alloy 152 heat WC04F6 (top left) specimen, two Alloy 152 heats 720129 and 146444 in succession (bottom) specimen, and an Alloy 152 heat 720129 in a 1st layer configuration specimen were machined. This last specimen was the focus of this year's testing effort. The data for the non-aged material is provided in Figure 5.

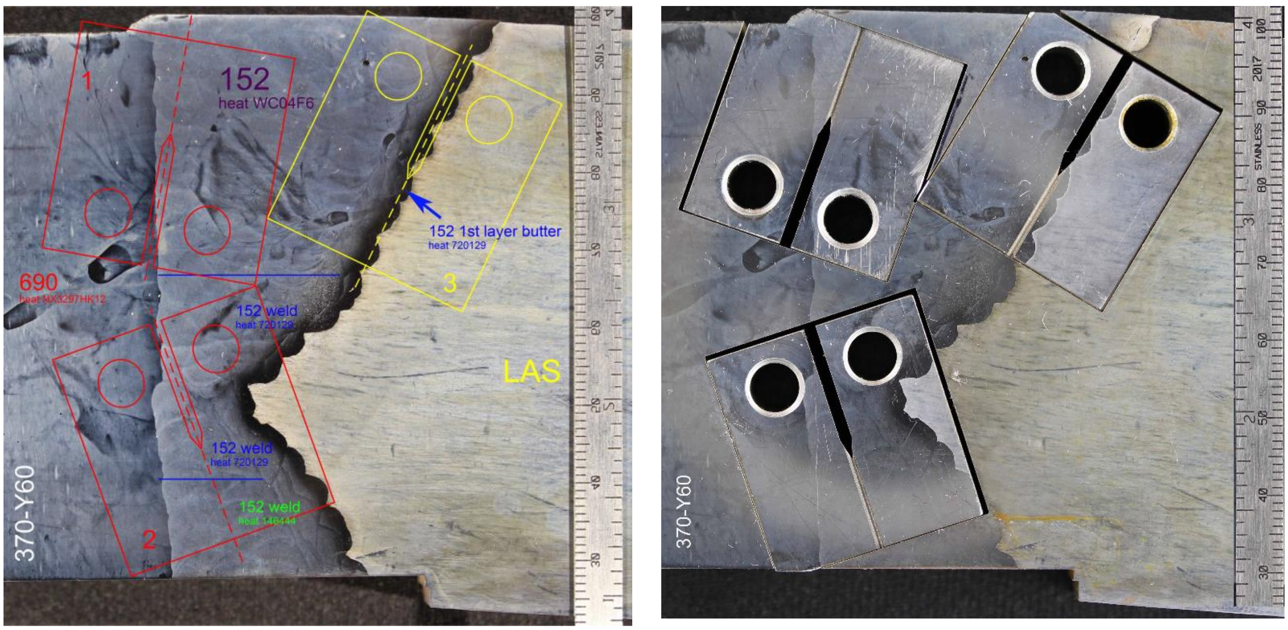

(a) (b)

Figure 27 a) Compact tension (CT) specimens designed to test the Alloy 152 heat WC04F6 (top left), Alloy 152 heats 720129 and 146444 in succession (bottom), and Alloy 152 heat 720129 in a 1st layer configuration. (b) CT specimens ready to be tested.

The testing conditions for Specimen 370-Y60 N152-LAS-11A are given in Table 8, and the changes in crack length and K_{max} with time are shown in Figure 28. The test was initiated with precracking in the environment, followed by successive fast (50s rise)/slow (600s rise) to advance and sample the environmental enhancement. As such, as the test progressed, the cyclic CGR response as well as the overall environmental enhancement and SCC CGR vs. crack advance (Figure 29) were monitored and used to inform the management of the test as described in Section 2.3.2.

Figure 29 shows that the environmental enhancement in the aged specimen never reached the level associated with extensive IG engagement. Indeed, the CGR response under cycle + 2h hold in test periods 7, 10, and 15 similar to that of the unaged specimen. The most promising rate observed in test period 15, was also confirmed at constant load in test period 16 to be a moderate 1 x 10^{-11} m/s.

Table 8 Crack growth data in PWR water[a] for Alloy 152 1st layer weld butter Specimen 370-Y60 N152-LAS-11A aged for 74,808 h at 370°C

Test Period	Test Time, h	Temp., °C	Load Ratio R	Rise Time, s	Down Time, s	Hold Time, s	K_{max}, MPa·m$^{1/2}$	ΔK, MPa·m$^{1/2}$	CGR_{env}, m/s	Estimated CGR_{air}, m/s	Crack Length, mm
Pre a	5	320.2	0.30	1	1	0	26.5	18.6	2.81E-08	8.20E-08	12.075
Pre b	23	320.1	0.30	50	50	0	26.7	18.7	1.18E-09	1.68E-09	12.117
Pre c	25	320.1	0.30	1	1	0	26.9	18.8	3.69E-08	8.67E-08	12.176
1	31	320.1	0.50	50	12	0	27.0	13.5	9.45E-10	7.59E-10	12.201
2	48	320.1	0.50	600	12	0	27.0	13.5	1.05E-10	6.37E-11	12.209
3	52	320.3	0.50	50	12	0	27.0	13.5	8.83E-10	7.69E-10	12.221
4	70	320.4	0.50	600	12	0	27.1	13.5	1.37E-10	6.44E-11	12.229
5	97	320.5	0.50	50	12	0	27.3	13.7	1.02E-09	8.07E-10	12.308
6	145	320.5	0.50	600	12	0	27.4	13.7	1.18E-10	6.76E-11	12.330
7	216	320.4	0.50	600	12	7,200	27.4	13.7	1.11E-11	5.19E-12	12.336
8	264	320.3	0.50	50	12	0	27.8	13.9	1.01E-09	8.67E-10	12.471
9	335	320.2	0.50	600	12	0	28.0	14.0	1.42E-10	7.42E-11	12.508
10	404	319.9	0.50	600	12	7,200	28.1	14.0	4.83E-12	5.74E-12	12.510
11	762	320.7	1.00	0	0	0	28.0	0.0	6.80E-12	-	12.517
12	821	320.5	0.50	600	12	0	28.0	14.0	1.28E-10	7.41E-11	12.547
13	870	320.6	0.50	50	12	0	28.4	14.2	6.31E-10	9.39E-10	12.629
14	894	320.4	0.50	600	12	0	28.5	14.2	1.49E-10	7.92E-11	12.643
15	1,063	319.9	0.50	600	12	7,200	28.5	14.3	2.00E-11	6.13E-12	12.657
16	1,474	319.9	1.00	0	0	0	28.4	0.0	1.05E-11	-	12.673

[a]Simulated PWR water with 2 ppm Li, 1000 ppm B, and 2 ppm H. DO<10 ppb. Conductivity is 21±3 µS/cm, and pH is 6.4.

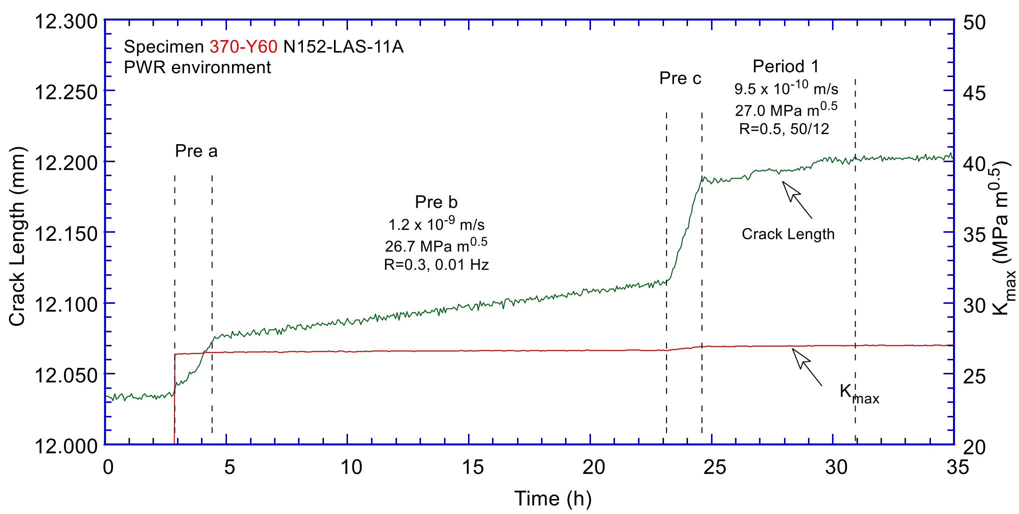

(a)

Figure 28 Crack length vs. time in simulated PWR environment for Alloy 152 1st layer weld butter Specimen 370-Y60 N152-LAS-11A aged for 74,808 h at 370°C, during test periods: (a) precracking-1, (b) 2-7, (c) 8-11, and (d) 12-16.

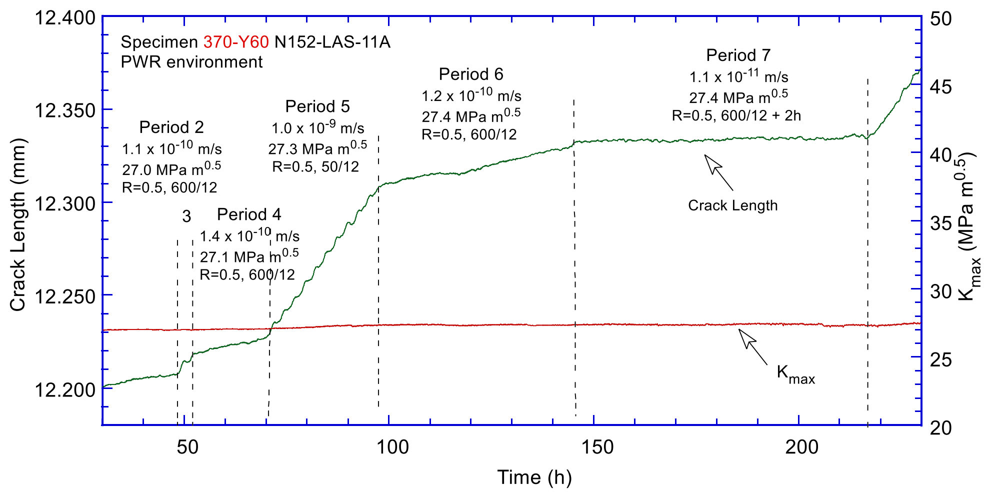

(b)

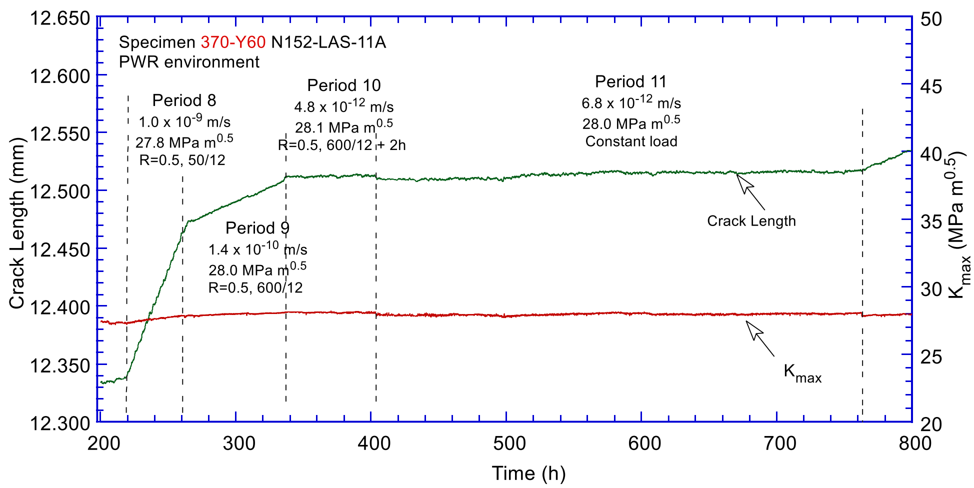

(c)

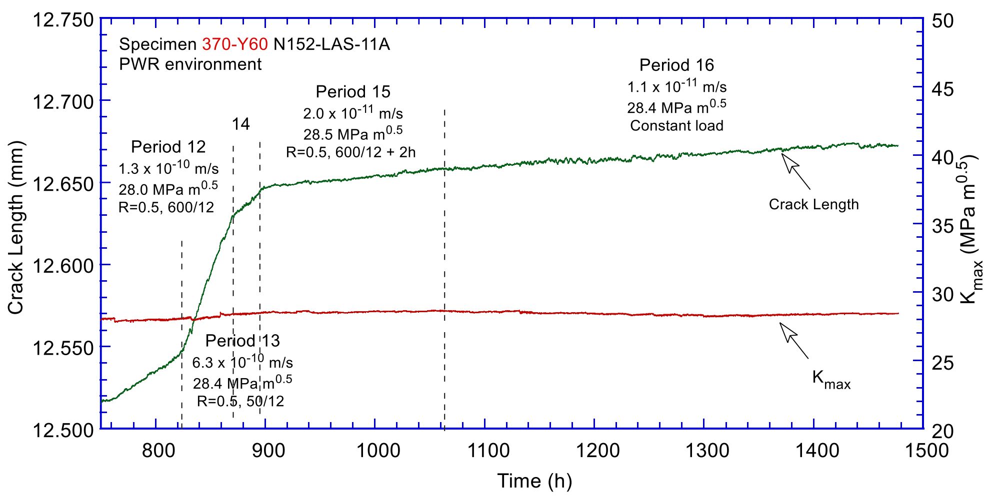

(d)

Figure 28 (cont.)

The environmental enhancement of two cyclic CGRs as well as the SCC CGRs vs. distance from the specimen notch are shown in Figure 29 for un-aged Specimen N152-LAS-11 (not corrected DC potential data), and (b) Specimen 370-Y60 N152-LAS-11A aged to an equivalent of 60 years of service. As described previously, the environmental enhancement in the aged specimen never reached the level associates with extensive IG engagement (red dotted line in the figure).

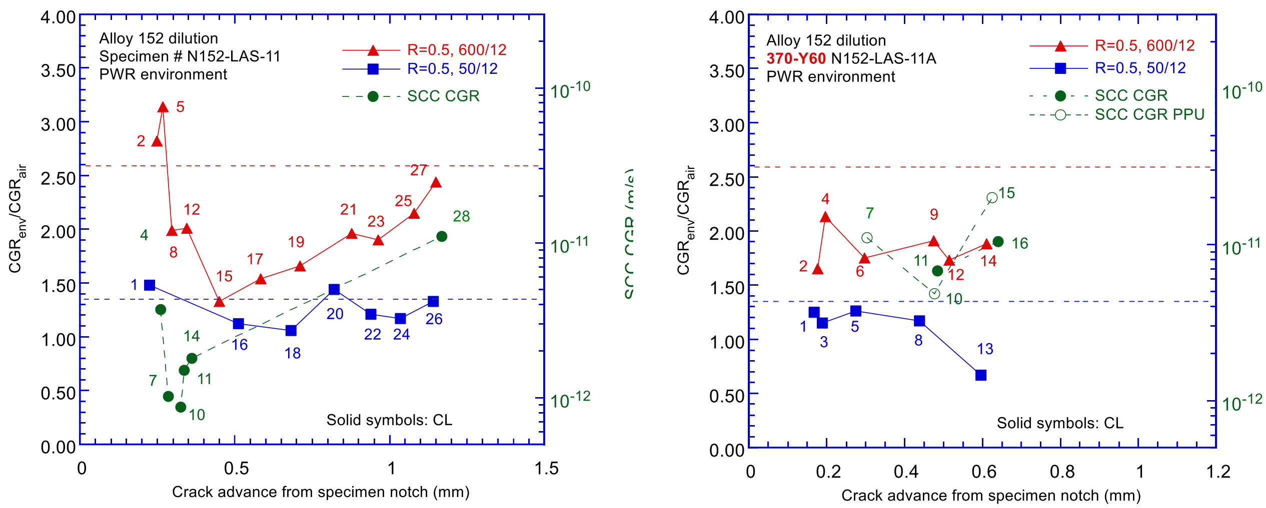

(a) (b)

Figure 29 Environmental enhancement of the cyclic CGRs and SCC CGRs vs. distance from the notch for (a) un-aged Specimen N152-LAS-11 (not corrected), and (b) Specimen 370-Y60 N152-LAS-11A aged to an equivalent of 60 years of service.

4 Discussion

This section provides summary of the aging effects in Alloy 152 as a weldment and as a 1st layer weld butter deposited on LAS and discusses the potential implications on performance. The testing results of aged alloys are discussed in the framework provided by the well-established fatigue and corrosion fatigue behavior for these alloys, as well as the industry-proposed disposition curves for crack growth.

4.1 Effects of aging on microstructure of Alloy 152

Weldments, including weld butter layers, add complexity when compared to the base alloys. Grain morphology, retained internal stress, segregation, precipitates, etc., are all factors that may evolve with service time and affect the formation of ordered phases, such as LRO, by altering the local diffusivity. In turn, local diffusivity and microstructure will also be impacted in varying degrees depending on the location in the weld. Moreover, both microstructure and ordered phases can affect SCC.

The location of analysis within a weld is expected to play a role and potentially affect local diffusivity and outcomes of the microstructural investigations and analyses. Hence, as described in this report, a "finer" microstructural characterization by means of synchrotron X-ray was conducted in small, 0.2 mm - step line scans in the high-deformation regions of the weld root – covering areas spanning from the weld heat affected zone (HAZ) in Alloy 690 to the weld and weld butter on LAS. This investigation did not find evidence of LRO in any of the Alloy 152 heats aged at 370°C and 450°C to an equivalent of 60 years of service.

While LRO and its effect on SCC response is one of the main questions that this research is attempting to answer, it is important to keep in mind that the microstructural effects of thermal aging have been studied extensively in the past, leading to a comprehensive understanding of thermally-induced Cr carbide precipitation along grain boundaries [29], further resulting into an overall increase in hardness. From an SCC susceptibility standpoint, Cr carbide precipitation depletes Cr at grain boundaries [29], and thus could potentially decrease resistance to SCC. Moreover, a recent analysis included in this report found evidence of carbide coarsening with aging. The coarsening of grain boundary carbides can lead to higher local stress concentrations, which can cause localized rupture and microcrack formation [30]. In essence, an increase in hardness, whether due to LRO formation or Cr-carbide precipitation and coarsening, can potentially have a negative effect on the SCC resistance, and hence needs to be investigated experimentally. The SCC CGR testing undertaken in this program and presented in this report addresses that need.

The weld butter, investigated in this study, has two heats and both have Fe content < 10 wt. %, making them more susceptible to LRO. The second butter layer was found resistant to SCC [19] in the as-welded condition, hence the microstructure evolution will likely determine whether this layer develops SCC-susceptibility with aging. The first layer was already highly susceptible to SCC (Figure 5), and has Fe content < 10 wt. %. Even without LRO, this layer has abundant Type-II boundaries that are potential SCC paths [20]. As described previously, the coarsening of the carbides at those boundaries would lead to higher local stress concentrations, thus increasing the susceptibility to SCC. Of even higher concern are the regions between the fusion line with the LAS and the Type-II boundaries. As presented in Section 3.1.3, these areas have been observed to increase in hardness with aging from already high levels; the extreme hardening with aging ($\Delta HV \cong 100$) was further confirmed at two locations within the weldment. Moreover, the coarsening of grain boundary carbides in the LAS HAZ has the potential to transform this region from largely SCC-resistant [19] to SCC-susceptible. Overall, it seems that the regions adjacent to the first layer weld butter weld - LAS interface have the potential to become SCC-susceptible paths with aging even in the absence of LRO. LRO, if it were to also develop with aging, would likely increase the SCC susceptibility over that of the aged material without LRO.

4.2 Effects of aging on crack growth response of Alloy 152 Heat 720129

Alloy 152 Heat 720129 was used in both the J-weld and the weld butter deposited on LAS. Both weld and weld butter specimens were tested in the non-aged and aged conditions. In order to achieve the 60 years of service equivalent, the weldments were aged at 370°C for 74,808 h. This section summarizes and discusses the cyclic and SCC CGR results for the two weldments.

4.2.1 Cyclic and SCC CGR response of aged Alloy 152 Heat 720129

Figure 30 summarizes the cyclic and SCC CGR data for aged Alloy 152 Heat 720129 [14]. Figure 30a presents the cyclic CGR data obtained on Alloy 152 heat 720129 in the as-welded and aged conditions. In the figure, the cyclic CGRs measured in the environment are plotted vs. the CGRs predicted in air under the same loading conditions for Ni-based weldments [33, 34]. In this representation, the environmental enhancement, i.e., the departure from the "1:1 diagonal" can be easily visualized. For comparison, the cyclic CGR curve for Alloy 182 weld was also included [35-37]. Figure 30a shows that the cyclic CGRs in the mechanical fatigue regime (10^{-8}-10^{-7} m/s) are as expected, i.e., close to the first diagonal. Likewise, in the corrosion fatigue regime (10^{-11}-10^{-9} m/s), there is no difference between the aged and non-aged specimens. Also, unsurprisingly, at the lower end of the spectrum, the environmental enhancement of all Alloy 152 specimens is lower than the Alloy 182 curve – likely an effect of the higher Cr content than that of Alloy 182. Figure 30b presents the SCC CGR data for the aged Alloy 152 heat 720129 vs. stress intensity factor, K. In the non-aged condition, this alloy heat was only tested as a 1st layer butter on LAS [18], thus the SCC CGR data from the Cr-depleted (24-25%) version of this heat was deemed to be un-suitable for comparison in this context. Also, the proposed disposition curves for Alloys 182 [1] and 52/152 [2] are included in the figures. The SCC CGR data for the 60-year aged Alloy 152 heat 720129 is approximately a factor 20 higher than the EPRI MRP-386 [2] proposed disposition curve for high-Cr Ni-based weldments.

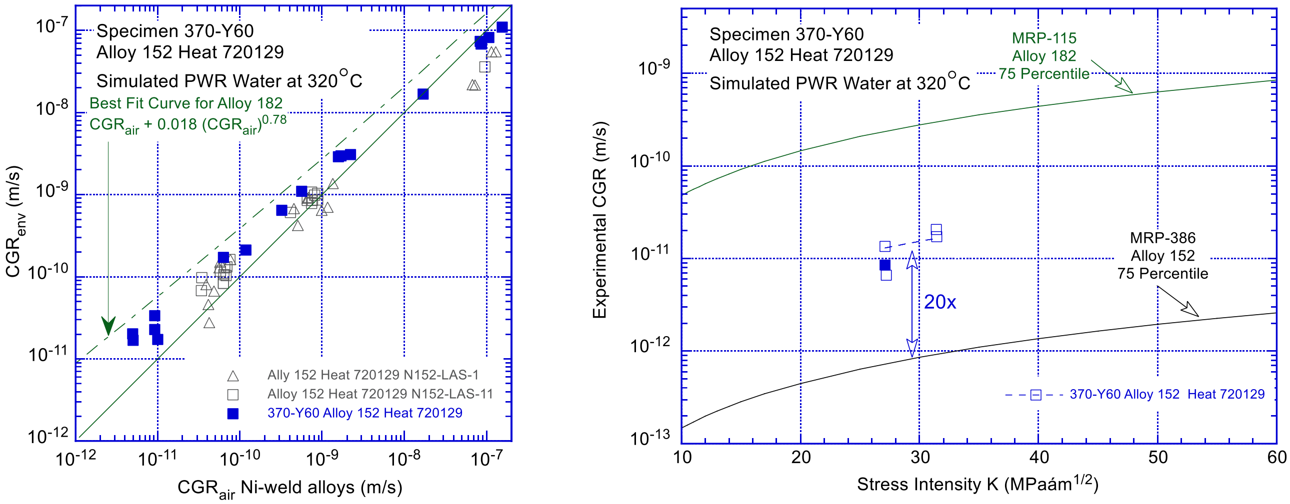

(a) (b)

Figure 30 (a) Cyclic CGRs measured in the environment vs. CGRs predicted in air under the same loading conditions, and (b) SCC CGRs for Alloy 152 weld heat 720129 in the 60-year aged condition. The available cyclic CGR data for the unaged condition [17, 19] was included for coparison. For SCC CGRs, solid symbols represent measurements under constant load (CL) and open symbols represent measurements under periodic partial unloading (PPU) conditions. The proposed disposition curves for Alloys 182 [1] and 52/152 [2] are included.

4.2.2 Cyclic and SCC response of aged 1st Layer Alloy 152 Heat 720129 deposited on LAS

Figure 31 summarizes the cyclic and SCC CGR data for aged 1st Layer Alloy 152 Heat 720129 deposited on LAS, and provides a comparison with a non-aged version of this alloy. Figure 31a presents the cyclic CGR data obtained on Alloy 152 Heat 720129 deposited as 1st layer in the non-aged and aged conditions. Figure 31a shows the cyclic CGRs measured in the environment plotted vs. the CGRs predicted in air under the same loading conditions for Ni-based weldments [33, 34]. For comparison, the cyclic CGR curve for Alloy 182 weld was also included [35-37]. Figure 31a shows that, for the aged specimen, the cyclic CGRs in the mechanical fatigue regime (10^{-8}-10^{-7} m/s) are exactly as expected, i.e., along the first diagonal. In the corrosion fatigue regime (10^{-11}-10^{-9} m/s), there is no difference between the aged and non-aged specimens. Figure 31b presents the SCC CGR data for Alloy 152 Heat 720129 deposited as a 1st layer on LAS in both aged and non-aged conditions vs. stress intensity factor, K. Also included are the proposed disposition curves for Alloys 182 [1] and 52/152 [2]. The SCC CGR data for the 60-year aged Alloy 152 Heat 720129 deposited as a 1st layer on LAS does not appear to show a deterioration with aging.

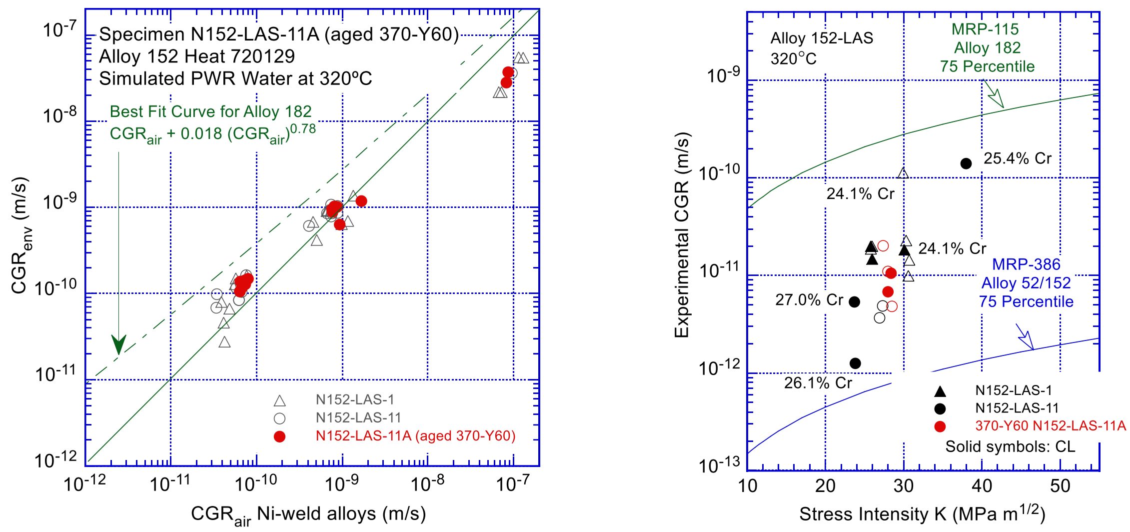

(a) (b)

Figure 31 **(a) Cyclic CGRs measured in the environment vs. CGRs predicted in air under the same loading conditions, and (b) SCC CGRs for Alloy 152 1st layer weld butter Specimen 370-Y60 N152-LAS-11A in the as-received [17, 19], and aged conditions. For SCC CGRs, solid symbols represent measurements under constant load (CL) and open symbols represent measurements under periodic partial unloading (PPU) conditions. The proposed disposition curves for Alloys 182 [1] and 52/152 [2] are included.**

4.2.3 Data interpretation challenges and potential solutions

One of the major outcomes of the research effort is that the extreme hardening with aging of ΔHV ≅ 100 in the 1st layer Alloy 152 weld butter did not appear to result in a substantial increase in the SCC CGR response. One potential explanation may have to do with the duration and extent of the test. As such, Figure 29 shows that in the non-aged material, the crack was advanced for approximately 1 mm to reach two regions of high environmental enhancement, i.e., high IG engagement. By contrast, in the aged specimen, less than half material was sampled, and no region of high IG engagement was reached. The results suggest that large ΔHV may affect only cases where the crack propagation mode is IG. This observation is substantiated by the fact that cyclic CGRs did not seem to be affected in any of the aged materials that were tested in this program. One way to reduce the uncertainty would be to continue testing the same specimen after additional aging; for this purpose, Specimen 370-Y60 N152-LAS-11A is currently additionally aged to 100 years of service.

Another consideration has to do with the availability of the Type-II boundaries for crack propagation. While such boundaries appear to be abundant in the unaged material (Figure 17), the effect of aging on this network of boundaries is less clear. While there is evidence that aging affects the spacing between the fusion boundary and the nearest Type II, as well as the stress levels of these regions [22, 38], these effects have not been quantified in a systematic fashion.

5 Conclusions

The need for an assessment of the long term aging effects on the performance of Alloy 690 and associated weldments was identified as a research gap in the LWRS stakeholders report for 2020 [9], being recognized as such by both industry [2, 10] and regulators [11]. The research undertaken in this program is addressing that gap. Specifically, the work focused on the microstructural evolution and the SCC response of Alloy 152 following accelerated thermal aging. The materials studied involved Alloy 152 deposited as a 1st layer butter on LAS, aged at three different temperatures (370°C, 400°C and 450°C) for up to 75,000h. The conclusions of this research are as follows:

- For three heats of Alloy 152 weld, aging at 370°C and 450°C to 60 year equivalent service did not find evidence of LRO. Additional, detailed microstructural characterization by means of synchrotron X-ray conducted in small, 0.2 mm - step line scans in the high-deformation regions of the weld root – covering areas spanning from the weld heat affected zone (HAZ) in Alloy 690 to the weld and weld butter on LAS – substantiated these findings.
- While LRO was not found, the effect of aging on hardening is less clear. Aging to an equivalent of 60 years of service did not appear to cause an increase in average hardness in the bulk welds, with the possible exception of the weld root area where hardness appears to increase slightly with aging.
- For the 1st layer Alloy 152 weld butter, the regions between the fusion line with the LAS and the Type-II boundaries were found to increase in hardness with aging from already high levels; the extreme hardening with aging was $\Delta HV \cong 100$. These regions remain of highest concern with respect to susceptibility to SCC.
- The aging temperature, 370°C or 450°C, does not seem to affect the findings. In absence of LRO, hardening is suspected to be due to thermally-induced Cr carbide precipitation and coarsening. Carbide precipitation depletes Cr at grain boundaries [29], thus potentially decreasing the resistance to SCC. The coarsening of grain boundary carbides can lead to higher local stress concentrations, which can cause localized rupture and microcrack formation [30]. The SCC CGR testing undertaken in this program and presented in this report addresses those potential concerns.
- Testing in a primary water environment of Alloy 152 deposited as a 1st layer weld butter on LAS, aged at 370°C to a 60-year service equivalent revealed fatigue and corrosion fatigue crack growth responses similar to those measured on the un-aged alloy.
- The SCC CGR data for 60-year aged Alloy 152 deposited as a 1st layer weld butter on LAS does not seem to show deterioration of the SCC performance. The analysis of the environmental enhancement of the cyclic CGRs suggests that the IG engagement of the aged specimen was not as high as that obtained in the test on the non-aged specimen. To reduce uncertainty, further CGR testing on the same specimen after additional aging is planned.

References

1. Materials Reliability Program: Crack Growth Rates for Evaluating Primary Water Stress Corrosion Cracking (PWSCC) of Alloy 82, 182, and 132 Welds (MRP-115), EPRI, Palo Alto, CA: 2004. 1006696.
2. Electric Power Research Institute, "Recommended Factors of Improvement for Evaluating Primary Water Stress Corrosion Cracking (PWSCC) Growth Rates of Thick-Wall Alloy 690 Materials and Alloy 52, 152, and Variants Welds (MRP-386)," Palo Alto, CA, 2017: 3002010756.
3. Young, G.A., Morton, D.S., Lewis, N. Morris, R., Pyle, J., Barnard, L., Najafabadi, R., Effect of Long Range Order on the Stress Corrosion Susceptibility of a Nickel-33 at% Chromium Alloy, Corrosion 72 2016 1433.
4. Marucco, A., Atomic Ordering in the Ni-Cr-Fe system, Mat. Sci. and Eng. A189 (1994) 267.
5. F. Delabrouille, D. Renaud, F. Vaillant, J. Massoud, Long range ordering of Alloy 690, in: 14th. Int. Conf. On Environmental Degradation of Materials in Nuclear Power Systems, 2009, pp. 888-894.
6. Brimbal, D., Joly, P., Benhamou, C., Thermal aging of Ni-Cr and Ni-Cr-Fe alloys to determine the potential for long-range ordering of Alloy 690 at PWR relevant temperatures, EPRI PWSCC Research Collaboration Meeting 2019, Tampa, Florida, December 4th, 2019.
7. Houtilainen, C., Ehrnstén, U., Ahonen, M., Hänninen, H., Effect of Thermal Aging on Microstructure and Hardness of Industrial Heats of Alloy 690, 19th. Int. Conf. On Environmental Degradation of Materials in Nuclear Power Systems, 2019.
8. Song, M., Yang, Y., Wang, M., Kuang, W., Lear, C.L., Was, G.S., Probing long-range ordering in nickel-base alloys with proton Irradiation, Acta Materialia 156 (2018) 446-462.
9. Light Water Reactor Sustainability Program Stakeholder Engagement Meeting Summary Report, INL/EXT-19-54520, February, 2020.
10. Burke, M., Coordination of EPRI Issue Programs' Research Activities with LWRS Materials Pathway Projects, LWRS Materials Research Pathway Stakeholder Engagement Meetings, August 18, 2020.
11. Collins, J., and Focht, E., Nickel-Based Alloy Crack Growth Rates, Industry / NRC Materials Programs Technical Information Exchange, August 11, 2021, ML21217A260.
12. Alexandreanu, B., Chen, Y., Zhang, X., and W. Y. Chen, "Effect of Thermal Aging and Irradiation on Microstructure and Crack Growth Response in Alloy 690," ANL/LWRS- 21/1, September 2021.
13. Alexandreanu, B., Chen, Y., Zhang, X., and W. Y. Chen, "Effect of Thermal Aging and Irradiation on Microstructure and Crack Growth Response in Alloy 152 Weld," ANL/LWRS- 22/2, September 2022.
14. Alexandreanu, B., Chen, Y., Zhang, X., and W. Y. Chen, "Effect of Thermal Aging on Microstructure and Stress corrosion Cracking Behavior of Alloy 152 weldments," ANL/LWRS- 23/1, September 2023.
15. Material Documentation Report for Consumers Power Midland (620-0012-51) and TMI-2 (620-0006-51) Reactor Vessel Lower Head Material, The Babcock & Wilcox Company, BAW-2071, January 1989.
16. Dunn, D., Alexandreanu, B., Toter, W., "Shielded Metal Arc Welding Parameters for Primary Water Stress Corrosion Cracking Test Materials," Technical Letter Report ML13171A113, June 2013.
17. Alexandreanu, B., Y. Yang, Y. Chen, and W. J. Shack, "Stress Corrosion Cracking in Nickel-Base Alloys 690 and 152 Weld in Simulated PWR Environment - 2009," NUREG/CR–7137, ANL–10/36, June 2012.

18. Alexandreanu, B., Chen, Y., Natesan, K., and Shack, “Primary Water Stress Corrosion Cracking of High-Chromium, Nickel-Base Welds Near Dissimilar Metal Weld Interfaces,” NUREG/CR–7226, ANL–16/10, January 2018.
19. Alexandreanu, B., Chen, Y., Natesan, K., and Shack, “Primary Water Stress Corrosion Cracking of High-Chromium, Nickel-Base Welds - 2018,” NUREG/CR–7276, 2021.
20. Alexandreanu, B., Chen, Y., Natesan, K., and Shack, “Primary Water Stress Corrosion Cracking of High-Chromium Nickel-Base Welds at or Near Interfaces – 2020,” NUREG/CR–7277, 2023.
21. Choi, K.J., Kim, J.J, Bong, H.L., Bahn, C.B., Kim, J.H., Effects of thermal aging on microstructures of low alloy steel–Ni basealloy dissimilar metal weld interfaces, Journal of Nuclear Materials 441 (2013) 493-502.
22. Yoo, S.C., Choi, K.J., Bahn, C.B., Kim, S.H., Kim, J.Y., Kim, J.H., Effects of thermal aging on the microstructure of Type-II boundaries in dissimilar metal weld joints, Journal of Nuclear Materials 459 (2015) 5-12.
23. B. Alexandreanu, B. Capell and G.S. Was, Combined Effect of Special Grain Boundaries and Grain Boundary Carbides on IGSCC of Ni-16Cr-9Fe-xC Alloys, *Mat. Sci. and Eng.* A 300 (2001) 94.
24. Gwalani, B., Alam, T., Miller, C., Rojhirunsakool, T., Kim, Y.S., Kim, S.S., Kaufman, M., Ren, Y., and Banerjee, R., (2016). Experimental investigation of the ordering pathway in a Ni-33 at.%Cr alloy. Acta Materialia. 115. 372-384. 10.1016/j.actamat.2016.06.014.
25. American Society for Testing and Materials, “Standard Test Method for Measurement of Fatigue Crack Growth Rates,” ASTM E647-08, DOI 10.1520/E0647-08, West Conshohocken, PA, 2008.
26. American Society for Testing and Materials, “Standard Test Method for Determining a Threshold Stress Intensity Factor for Environment-Assisted Cracking of Metallic Materials,” ASTM E1681-03, DOI 10.1520/E1681-03R08, West Conshohocken, PA, 2008.
27. Electric Power Research Institute, “PWR Primary Water Chemistry Guidelines,” Volume 1, Revision 4, EPRI, Palo Alto, CA, 1999.
28. Alexandreanu, B., Zhang, X., Chen, W. Y., and Y. Chen, “The Effect of Thermal Aging on the Performance of High-Cr Ni-based Alloys in Primary Water Environment, Part 1: Microstructure”, ANL/NSE- 23/71, 2023.
29. Angeliu, T.M., and Was, G.S., Behavior of grain boundary chemistry and precipitates upon thermal treatment of controlled purity Alloy 690, Metall. Trans. A 21A, 2097 (1990).
30. Hertzberg, R.W., Deformation and fracture mechanics of engineering materials, John Wiley, Inc., 1976.
31. Nelson, T.W., Lippold, J.C., and Mills, M.J., Nature and Evolution of the Fusion Boundary in Ferritic-Austenitic Dissimilar Metal Welds — Part 2: On-Cooling Transformations, Supplement to the Welding Journal, October 2000, 267.
32. Hou, J., Peng, Q., Takeda Y., Jiro, K., Shoji, T., Microstructure and stress corrosion cracking of the fusion boundary region, in an alloy 182-A533B low alloy steel dissimilar weld joint, Corrosion Science 52 (2010) 3949–3954.
33. Ruther, W. E., W. K. Soppet, and T. F. Kassner, “Corrosion Fatigue of Alloys 600 and 690 in Simulated LWR Environments,” NUREG/CR-6383, ANL-95/37, April 1996.
34. Ruther, W. E., W. K. Soppet, T. F. Kassner, and W. J. Shack, “Environmentally Assisted Cracking of Alloys 600 and 690 in Simulated LWR Water,” in Environmentally Assisted Cracking in Light Water Reactors, Semiannual Report, January 1998-July 1998, NUREG/CR-4667, Vol. 26, ANL-98/30, pp. 25-32, March 1999.

35. Chopra, O. K., W. K. Soppet, and W. J. Shack, "Effects of Alloy Chemistry, Cold Work, and Water Chemistry on Corrosion Fatigue and Stress Corrosion Cracking of Nickel Alloys and Welds," NUREG/CR-6721, ANL-01/07, April 2001.
36. Alexandreanu, B., O. K. Chopra, and W. J. Shack, "Crack Growth Rates of Nickel Alloys from the Davis-Besse and V. C. Summer Power Plants in a PWR Environment," NUREG/CR–6921, ANL–05/55, November 2006.
37. Alexandreanu, B., O. K. Chopra, and W. J. Shack, "Crack Growth Rates of Nickel Alloy Welds in a PWR Environment," NUREG/CR–6907, ANL–04/3, May 2006.
38. Ahonen, M., Mouginot, R., Sarikka, T., Lindqvist, S., Que, Z., Ehrnstén, U., Virkkunen, I., and H. Hänninen, Effect of Thermal Ageing at 400°C on the Microstructure of Ferrite-Austenite Interface of Nickel-Base Alloy Narrow-Gap Dissimilar Metal Weld, Metals 10 (2020) 421.

This page intentionally left blank

Nuclear Engineering Division
Argonne National Laboratory
9700 South Cass Avenue, Bldg. 208
Argonne, IL 60439

www.anl.gov